

# Inviscid Burgers as a degenerate elliptic problem

Uditnarayan Kouskiya\*      Amit Acharya†

## Abstract

We demonstrate the feasibility of a scheme to obtain approximate weak solutions to the (inviscid) Burgers equation in conservation and Hamilton-Jacobi form, treated as degenerate elliptic problems. We show different variants recover non-unique weak solutions as appropriate, and also specific constructive approaches to recover the corresponding entropy solutions.

## 1 Introduction

In this paper we continue, following [1], the assessment of a recently introduced duality based approach to solving differential equations involving evolution in time. A nonlinear ODE system was considered in [1] (along with some linear PDE); here we consider the (inviscid) Burgers equation in conservation and Hamilton-Jacobi form.

Our essential idea (see App. A) is to treat the primal PDE under consideration as constraints and invoke a more-or-less arbitrarily designable strictly convex, auxiliary potential to be optimized. Then, a dual variational principle for the Lagrange multiplier (dual) fields can be designed involving a dual-to-primal (DtP) mapping (i.e. an adapted change of variables), with the special property that its Euler-Lagrange equations are exactly the primal PDE system, interpreted as equations for the dual fields using the DtP mapping, and this, even though the primal system may not have the required symmetries necessary to be the Euler-Lagrange equations of any objective functional of the primal fields alone. We use a simple Galerkin Finite element discretization of the dual Euler-Lagrange system (which is the primal system of interest using a change of variables) to look for a computational approximation of weak solutions to (inviscid) Burgers equation. The system is degenerate-elliptic in space-time domains.

To our knowledge, our approach for generating approximate solutions to a nonlinear hyperbolic problem (albeit scalar here, but seamlessly generalizable to systems, formally at least) is new. Brenier [2, Sec. 4] solves the inviscid Burgers problem without approximation through a maximization of a functional related to ours, but without the use of ‘base states,’ (see Sec. 2 and App. B) which we find crucial in making our ideas work; in fact, we have to employ a sequence of dual functionals parametrized by evolving base states, the latter self-consistently prescribed by the scheme. As very nicely explained by a ‘safe mountain climbing’ analogy, Brenier’s exact scheme [2, Sec. 4] is different from our approach, and computational results are shown in [3, pp.101-105]; he also established connections to an Optimal Transport based method of attack, which can be utilized for computational approximations via the celebrated Benamou-Brenier formulation of optimal transport theory, as mentioned in [2, Sec. 4.1, p. 597].

---

\*Department of Civil & Environmental Engineering, Carnegie Mellon University, Pittsburgh, PA 15213, email: udk@andrew.cmu.edu.

†Department of Civil & Environmental Engineering, and Center for Nonlinear Analysis, Carnegie Mellon University, Pittsburgh, PA 15213, email: acharyaamit@cmu.edu.

An outline of the paper is as follows: Sec. 2 and Sec. 3 comprise the development of the weak formulation for the dual inviscid Burgers equation in conservation and Hamilton-Jacobi forms, respectively. Sec. 4 describes the algorithm for the results computed in the paper. In Sec. 5, five selected problems are solved to illustrate and evaluate the features of the formulation and algorithm developed in Sections 2 and 3, as they relate to generating approximate solutions to the (inviscid) Burgers equation. The paper also contains five appendices supporting various sections of the main narrative. A word on notation: we always use the Einstein summation convention for indices unless otherwise mentioned and except when the indices are  $x, t$ .

## 2 Dual formulation of the Burgers Equation

Burgers equation [4, 5] is a (convection-dominated) convection-diffusion partial differential equation given by

$$\partial_t u + u \partial_x u = \nu \partial_{xx} u \quad \text{in } \Omega, \quad (1)$$

where  $\Omega = (0, L) \times (0, T) \in \mathbb{R} \times \mathbb{R}^+$  is a domain in (1-d)space-time,  $u : \Omega \rightarrow \mathbb{R}$  and  $\nu \in \mathbb{R}^+$  are the flow velocity and viscosity, respectively, in the context of fluid mechanics. A schematic of the

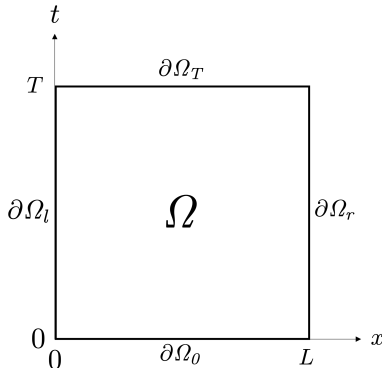


**Figure 1:** Domain of interest

domain is shown in Fig. 1. Henceforth,  $L = 1$ . The boundaries  $\partial\Omega_l$ ,  $\partial\Omega_r$ ,  $\partial\Omega_0$  and  $\partial\Omega_T$  will be referred to as the left, right, bottom and top boundaries, respectively.

We will be mainly interested in the inviscid Burgers equation, obtained by setting  $\nu = 0$  in (1):

$$\partial_t u + u \partial_x u = 0 \quad \text{in } \Omega,$$

and, as is standard, explore weak solutions of this quasilinear equation expressed in conservation form:

$$\partial_t u + \partial_x \left( \frac{1}{2} u^2 \right) = 0 \quad \text{in } \Omega, \quad (2)$$

with initial and the boundary conditions given by

$$u(x, 0) = u_0(x); \quad u(0, t) = u_l(t). \quad (3)$$

Following the ideas in Appendix A, we form the product of (2) with a dual field  $\lambda : \Omega \rightarrow \mathbb{R}$  (that acts like a Lagrange multiplier) and integrate by parts in the space-time domain to define a pre-dual

functional

$$\begin{aligned}\widehat{S}_H[u, \lambda] &= \int_{\Omega} \left( -u \partial_t \lambda - \frac{u^2 \partial_x \lambda}{2} + H(u, x, t) \right) dt dx - \int_0^L u_0(x) \lambda(x, 0) dx - \int_0^T u_l(t) \lambda(0, t) dt \\ &= \int_{\Omega} \mathcal{L}_H(u, \mathcal{D}, x, t) dt dx - \int_0^L u_0(x) \lambda(x, 0) dx - \int_0^T u_l(t) \lambda(0, t) dt,\end{aligned}$$

where  $\mathcal{D} := (\partial_t \lambda, \partial_x \lambda)$  and  $H(u, x, t)$  is a ‘free’ auxiliary potential. The design of the functional involves inclusion of only those space-time boundary terms that contain information available from the primal problem [6, 1]. Additionally, we impose the following Dirichlet space-time boundary conditions on  $\lambda$ :

$$\lambda(L, t) = \lambda_r(t); \quad (4a)$$

$$\lambda(x, T) = \lambda_T(x), \quad (4b)$$

where  $\lambda_r(t)$  and  $\lambda_T(x)$  can be specified arbitrarily. The choice of the auxiliary potential  $H$  needs to be such that it renders the following equation ‘solvable’ for  $u$  (Appendix A):

$$\frac{\partial \mathcal{L}_H}{\partial u} : -\partial_t \lambda - u \partial_x \lambda + \frac{\partial}{\partial u} H(u, x, t) = 0. \quad (5)$$

We employ the following shifted quadratic form for  $H(u, x, t)$

$$H(u, x, t) = \frac{\beta_u}{2} (u - \bar{u}(x, t))^2, \quad (6)$$

where  $\beta_u \gg 1$ . The function  $\bar{u} := \bar{u}(x, t)$ , is a ‘free’ function to choose that is referred to as a *base state* (see [6, Sec. 5]-[1, Sec. 4]). The choice of this base state is often crucial for the success of the scheme (see Appendix B for a simple example) and their algorithmic use is shown in [1, Sec. 5.3] and in Section 5 of this work, among others. Solving for  $u$  in (5), one obtains the following *dual-to-primal mapping* (DtP):

$$\begin{aligned}u^{(H)}(\mathcal{D}, x, t) &= \bar{u} + \frac{\bar{u} \partial_x \lambda + \partial_t \lambda}{\beta_u - \partial_x \lambda} \\ \hat{u}(x, t) &:= u^{(H)}(\mathcal{D}(x, t), x, t).\end{aligned} \quad (7)$$

The *dual* functional is now defined as

$$\begin{aligned}S_H[\lambda] := \widehat{S}_H[u^{(H)}(\mathcal{D}, x, t), \lambda] &= \int_{\Omega} \mathcal{L}_H(u^{(H)}(\mathcal{D}, x, t), \mathcal{D}, x, t) dt dx \\ &\quad - \int_0^L u_0(x) \lambda(x, 0) dx - \int_0^T u_l(t) \lambda(0, t) dt.\end{aligned} \quad (8)$$

The above functional can be explicitly written in terms of  $\lambda$  as

$$\begin{aligned}S_H[\lambda] &= \int_{\Omega} \mathbb{K}|_{\mathcal{D}} (\partial_t \lambda + \bar{u} \partial_x \lambda)^2 dt dx - \int_{\Omega} \left( \bar{u} \partial_t \lambda - \bar{u}^2 \frac{\partial_x \lambda}{2} \right) dt dx \\ &\quad - \int_0^L u_0(x) \lambda(x, 0) dx - \int_0^T u_l(t) \lambda(0, t) dt.\end{aligned} \quad (9)$$

where

$$\mathbb{K} = \frac{-1}{2\beta_u \left(1 - \frac{\partial_x \lambda}{\beta_u}\right)}.$$

Hence, for  $\beta_u \gg |\partial_x \lambda|$ , the nonlinear part of the bulk integrand is non-positive. The first variation of the above functional in a direction  $\delta \lambda$  yields

$$\begin{aligned} \delta^{(1)} S[\lambda; \delta \lambda] = & \int_{\Omega} \left( \frac{\partial \mathcal{L}_H}{\partial \hat{u}} \frac{\partial \hat{u}}{\partial \mathcal{D}_k} d\mathcal{D}_k + \frac{\partial \mathcal{L}_H}{\partial \mathcal{D}_k} d\mathcal{D}_k \right) dt dx - \int_0^L u_0(x) \delta \lambda(x, 0) dx \\ & - \int_0^T u_l(t) \delta \lambda(0, t) dt. \end{aligned}$$

The first term in the domain integral vanishes due to (5). Since  $\mathcal{L}_H$  is necessarily affine in  $\mathcal{D}$  one has

$$\begin{aligned} \delta^{(1)} S[\lambda; \delta \lambda] = & \int_{\Omega} \left( \partial_t \hat{u} + \frac{\partial}{\partial x} \left( \frac{\hat{u}^2}{2} \right) \right) \delta \lambda dt dx - \int_0^L \hat{u}(x, T) \delta \lambda(x, T) dx - \int_0^T \hat{u}(L, t) \delta \lambda(L, t) dt \\ & \int_0^L (\hat{u}(x, 0) - u_0(x)) \delta \lambda(x, 0) dx + \int_0^T (\hat{u}(0, t) - u_l(t)) \delta \lambda(0, t) dt, \end{aligned}$$

and using  $\delta \lambda$  consistent with (4), the E-L equations and side-conditions are given by

$$\partial_t \hat{u} + \frac{\partial}{\partial x} \left( \frac{\hat{u}^2}{2} \right) = 0 \quad \text{in } \Omega; \quad (10a)$$

$$\hat{u}(x, 0) = u_0(x); \quad \hat{u}(0, t) = u_l(t). \quad (10b)$$

which are simply (2)-(3) with the replacement  $u \rightarrow \hat{u}$ .

Thus, solutions of the problem defined by (2), (3) can be generated by solving (10) along with (4), where the DtP mapping (7) is utilized to bridge the primal variable  $u$  with the dual variable  $\lambda$ . In short, our scheme may be interpreted as designing an adapted *change of variables* for solving Burgers equation.

In [7], the degenerate ellipticity of the dual formulation of a significant class of equations from continuum mechanics is analyzed. We apply those ideas next to the dual formulation of Burgers equation given by (10) written as

$$\partial_t (\mathcal{F}_1(\hat{u})) + \partial_x (\mathcal{F}_2(\hat{u})) = 0,$$

some of whose analytical properties are governed by the terms

$$A_{ij} = \frac{\partial \mathcal{F}_i}{\partial (\nabla D)_j} = \frac{\partial \mathcal{F}_i}{\partial u} \Big|_{\hat{u}} \frac{\partial u}{\partial (\nabla D)_j},$$

where  $\nabla D := (\partial_t \lambda, \partial_x \lambda)$ , and

$$A_{11} = \frac{1}{\beta_u - \partial_x \lambda}; \quad A_{12} = \frac{\hat{u}}{\beta_u - \partial_x \lambda}; \quad A_{21} = \frac{\hat{u}}{\beta_u - \partial_x \lambda}; \quad A_{22} = \frac{\hat{u}^2}{\beta_u - \partial_x \lambda}.$$

Consequently, for  $\mathcal{D} = (0, 0)$

$$c_i A_{ij} c_j = \frac{(c_1 + \bar{u} c_2)^2}{\beta_u} \geq 0 \quad \forall (c_1, c_2) \in \mathbb{R}^2$$

which establishes that  $A_{ij}|_{\mathcal{D}=0}$  is positive semi-definite. Let  $\mathcal{N}$  be neighborhood around  $\mathcal{D} = (0, 0)$  and let  $\beta_u \gg |\partial_x \lambda|$ . Then, the following expression holds:

$$c_i A_{ij} c_j = \frac{(c_1 + \hat{u} c_2)^2}{\beta_u - \partial_x \lambda} = \frac{(c_1 + \hat{u} c_2)^2}{\beta_u \left( 1 - \frac{\partial_x \lambda}{\beta_u} \right)} \geq 0 \quad \forall (c_1, c_2) \in \mathbb{R}^2.$$

This relation establishes the positive semi-definiteness of  $A$  within this specific neighborhood. Consequently, the equation (10) is locally degenerate elliptic and for any surface with normal  $(n_1, n_2)$  in the space-time domain ( $n_1$  and  $n_2$  represents the projection of normal in the time and space directions, respectively), ellipticity fails when

$$(n_1, n_2) = \kappa(-\hat{u}, 1) \quad \text{for } \kappa \in \mathbb{R},$$

where  $\hat{u}$  is given by (7).

## 2.1 Weak formulation of the dual Burgers equation

A weak formulation of (10) with the side conditions (4) can be generated in the usual way through integration by parts or by considering the first variation of the functional (8) or (9) and setting it equal to zero. For any field  $\delta\lambda$  (within an appropriate class) satisfying the conditions stated below, we intend to find the dual field  $\lambda$  which satisfies the following equations:

$$\begin{aligned} R[\lambda; \delta\lambda] := \int_{\Omega} \left( -\hat{u} \partial_t \delta\lambda - \frac{\hat{u}^2 \partial_x \delta\lambda}{2} \right) dt dx - \int_0^L u_0(x) \lambda(x, 0) dx - \int_0^T u_l(t) \lambda(0, t) dt = 0; \\ \delta\lambda(x, T) = 0; \quad \delta\lambda(L, t) = 0; \\ \lambda(x, T) = \lambda_T(T); \quad \lambda(L, t) = \lambda_r(t), \end{aligned} \tag{11}$$

where  $\lambda_T(\cdot)$  and  $\lambda_r(\cdot)$  are arbitrarily specified functions satisfying  $\lambda_T(L) = \lambda_r(T)$ . The dual scheme formally guarantees that the solution to (11) implies the solution to the set of equations (10). We subsequently make use of the above weak form to numerically compute an approximate solution for the dual field and utilize the DtP mapping (7) to obtain the corresponding field for the primal problem i.e. the inviscid Burgers equation.

## 3 Dual formulation of the (inviscid) Burgers Equation in Hamilton-Jacobi form

Here we consider the Burgers equation (2) in Hamilton-Jacobi form:

$$\partial_t Y + \frac{(\partial_x Y)^2}{2} = \nu \partial_{xx} Y \quad \text{in } \Omega. \tag{12}$$

Differentiating (12) w.r.t.  $x$ , and defining  $\partial_x Y =: u$  gives (1). Throughout the following text, we will refer to this form of the Burgers equation as *Burgers-HJ* and when  $\nu = 0$ , we will refer to it as the *inviscid Burgers-HJ* equation. As already stated, our primary interest is in the inviscid case  $\nu = 0$ . We will consider the  $\nu \neq 0$  case to shed light on the inviscid case, the motivation for which will be provided in the relevant examples.

It is clear that (12) requires  $Y$  to be specified at one point of the domain, above and beyond information available from the corresponding Burgers equation. If the function  $u$  satisfies Burgers equation and  $\partial_x Y = u$  then  $\partial_t Y(x, t) + \frac{1}{2}u^2(x, t) - \nu \partial_x u(x, t) = f(x^*, t)$  for an arbitrarily fixed  $x^*$ , where  $f(x^*, t) = \partial_t Y(x^*, t) + \frac{1}{2}u^2(x^*, t) - \nu \partial_x u(x^*, t)$ . In all problems considered in the text and Appendix, we will always work with  $f(x^*, t) = 0$  with knowledge of the Burgers solution of interest known at the point  $x^*$  (mostly a boundary point) from which  $Y(x^*, t)$  is determined, with an initial condition  $Y(x^*, 0)$  arbitrarily specified.

The dual formulation of (12) for  $\nu = 0$  is obtained by writing it in first-order form [8, Sec. 6.2]:

$$\partial_t Y = -\frac{u^2}{2} \quad \text{in } \Omega; \quad (13a)$$

$$\partial_x Y = u \quad \text{in } \Omega. \quad (13b)$$

The initial and the boundary conditions can be given as

$$Y(x, 0) = Y_0(x); \quad Y(0, t) = Y_l(t). \quad (14)$$

Corresponding to the equations (13a) and (13b) we introduce the dual fields  $\lambda$  and  $\gamma$ , respectively. Similar to the setup explained in Sec. 2, we employ a shifted quadratic form for the auxiliary potential  $H$  in both  $Y$  and  $u$ :

$$H(Y, u, x, t) = \frac{\beta_Y}{2}(Y - \bar{Y})^2 + \frac{\beta_u}{2}(u - \bar{u})^2, \quad (15)$$

where  $\bar{Y}$  and  $\bar{u}$  correspond to the base states for  $Y$  and  $u$ , respectively.

With this choice of  $H$ , the DtP mapping for  $Y$  and  $u$ , given by  $Y^{(H)}$  and  $u^{(H)}$ , can be expressed in terms of the dual fields and their derivatives as

$$Y^{(H)}(\mathcal{D}, x, t) = \bar{Y} + \frac{\partial_t \lambda + \partial_x \gamma}{\beta_Y}; \quad (16a)$$

$$u^{(H)}(\mathcal{D}, x, t) = \bar{u} + \frac{\gamma - \lambda \bar{u}}{\beta_u + \lambda}, \quad (16b)$$

where  $\mathcal{D} := (\lambda, \gamma, \partial_t \lambda, \partial_x \gamma)$ . Additionally, the following boundary conditions are imposed:

$$\gamma(L, t) = \gamma_r(t); \quad (17a)$$

$$\lambda(x, T) = \lambda_T(x), \quad (17b)$$

where  $\gamma_r(t)$  and  $\lambda_T(x)$  can be specified arbitrarily. The *dual functional* obtained using the above procedure is

$$\begin{aligned} S_H[\lambda, \gamma] = \int_{\Omega} \left( -\hat{Y} \partial_t \lambda + \frac{\hat{u}^2 \lambda}{2} - \hat{Y} \partial_x \gamma - \hat{u} \gamma + H(\hat{Y}, \hat{u}, x, t) \right) dt dx \\ - \int_0^L Y_0(x) \lambda(x, 0) dx - \int_0^T Y_l(t) \gamma(0, t) dt, \quad (18) \end{aligned}$$

where

$$\hat{Y}(x, t) := Y^{(H)}(\mathcal{D}(x, t), x, t); \quad \hat{u}(x, t) := u^{(H)}(\mathcal{D}(x, t), x, t).$$

The functional above can be written explicitly in terms of the dual variables as

$$\begin{aligned} S_H[\lambda, \gamma] = \int_{\Omega} \left( -\frac{\mathbb{K}_1}{\beta_Y} (\partial_t \lambda + \partial_x \gamma)^2 - \frac{\mathbb{K}_2}{\beta_u} (\bar{u} \lambda - \gamma)^2 \right) dt dx \\ + \int_{\Omega} \left( \bar{Y} (\partial_t \lambda + \partial_x \gamma) + \bar{u} \left( \frac{\lambda \bar{u}}{2} - \gamma \right) \right) dt dx \\ - \int_0^L Y_0(x) \lambda(x, 0) dx - \int_0^T Y_l(t) \gamma(0, t) dt, \quad (19) \end{aligned}$$

where

$$\mathbb{K}_1 = \frac{1}{2}; \quad \mathbb{K}_2 = \frac{1}{2 \left(1 + \frac{\lambda}{\beta_u}\right)},$$

and for  $\beta_u \gg |\lambda|$ ,  $\mathbb{K}_2 > 0$ . Hence, the integrand containing nonlinear terms in the dual fields is negative semi-definite for this range of  $|\lambda|$ . The Euler-Lagrange equations of the dual functional (18), when extracted using the conditions (17), recover the primal equations (13) and (14), expressed in terms of their dual counterparts:

$$\partial_t \hat{Y} = -\frac{(\hat{u})^2}{2} \quad \text{in } \Omega; \quad (20a)$$

$$\partial_x \hat{Y} = \hat{u} \quad \text{in } \Omega;$$

$$\hat{Y}(x, 0) = Y_0(x); \quad \hat{Y}(0, t) = Y_l(t). \quad (20b)$$

Thus, a solution to the the above set of equations in dual variables implies a solution the primal problem using the DtP map (16).

To examine the ellipticity of the dual equations (20), we rewrite them as

$$\begin{aligned} \partial_t(\mathcal{F}_{11}(\hat{Y}, \hat{u})) + \partial_x(\mathcal{F}_{12}(\hat{Y}, \hat{u})) + \mathcal{G}_1(\hat{Y}, \hat{u}) &= 0; \\ \partial_t(\mathcal{F}_{21}(\hat{Y}, \hat{u})) + \partial_x(\mathcal{F}_{22}(\hat{Y}, \hat{u})) + \mathcal{G}_2(\hat{Y}, \hat{u}) &= 0, \end{aligned}$$

where  $\mathcal{F}_{12} = \mathcal{F}_{21} = 0$ . The behavior of the above set of equations is now governed by matrix

$$\mathbb{A}_{ijkl} = \frac{\partial \mathcal{F}_{ij}}{\partial (\nabla D)_{kl}}; \quad \nabla D = \begin{bmatrix} \partial_t \lambda & \partial_x \lambda \\ \partial_t \gamma & \partial_x \gamma \end{bmatrix},$$

with each of the indices  $i, j, k, l$  ranging from 1 to 2. Also,  $\mathbb{A}_{ijkl} = 0$  except

$$\mathbb{A}_{1111} = \mathbb{A}_{1122} = \mathbb{A}_{2211} = \mathbb{A}_{2222} = \frac{1}{\beta_Y}$$

Equivalently, we represent  $\mathbb{A}$  as a  $2 \times 2$  matrix  $A$ :

$$A = \begin{bmatrix} \mathbb{A}_{1111} & \mathbb{A}_{1112} & \mathbb{A}_{1121} & \mathbb{A}_{1122} \\ \mathbb{A}_{1211} & \mathbb{A}_{1212} & \mathbb{A}_{1221} & \mathbb{A}_{1222} \\ \mathbb{A}_{2111} & \mathbb{A}_{2112} & \mathbb{A}_{2121} & \mathbb{A}_{2122} \\ \mathbb{A}_{2211} & \mathbb{A}_{2212} & \mathbb{A}_{2221} & \mathbb{A}_{2222} \end{bmatrix} \quad (21)$$

which then satisfies

$$c_i A_{ij} c_j = \frac{(c_1 + c_4)^2}{\beta_Y} \geq 0 \quad \forall c \in \mathbb{R}^4,$$

establishing that  $\mathbb{A}_{ijkl}$  is positive semi-definite on the space of  $2 \times 2$  matrices and

$$C_{ij} \mathbb{A}_{ijkl} C_{kl} = 0 \quad \text{for } \{C \in \mathbb{R}^{2 \times 2} \mid C_{11} + C_{22} = 0\}.$$

Hence the equation set (20) is degenerate elliptic. Furthermore, for any rank-one matrix  $C$  of the form  $a \otimes n$  satisfying  $C : \mathbb{A}C = 0$ , for some  $a \in \mathbb{R}^2$  and some  $n \in \mathbb{R}^2, |n| = 1$ , the latter representing a unit normal in the space-time domain, the degenerate ellipticity (positive semi-definiteness of  $\mathbb{A}$ ) implies a loss of ellipticity along the direction  $n$ . Clearly, for any arbitrarily fixed unit normal  $n$ , there always exists a vector  $a$  such that  $a_1 n_1 = -a_2 n_2$ . As a result, ellipticity, i.e.  $\det(\mathbb{A}_{ijkl} n_j n_l) > 0$  fails along every unit normal in the domain (which is also apparent from the direct calculation  $\mathbb{A}_{ijkl} n_j n_l = \frac{1}{\beta_Y} n_i n_j$  which is a rank-one matrix).

### 3.1 Weak formulation for the dual Hamilton-Jacobi form of inviscid Burgers

We construct a weak form for the system of equations (20) with the side condition (17) in the usual way through integration by parts. As in the case of Burgers equation, the same weak form can also be obtained from the first variation of the dual functional (18) or (19). For any field  $\delta\lambda$  satisfying the conditions stated below, we intend to find the dual field  $\lambda$  which satisfies the following equations:

$$\begin{aligned}
 R[\lambda, \gamma; \delta\lambda, \delta\gamma] := & \int_{\Omega} \left( -\hat{Y} \partial_t \delta\lambda + \frac{\hat{u}^2 \delta\lambda}{2} - \hat{Y} \partial_x \delta\gamma - \hat{u} \delta\gamma \right) dt dx \\
 & - \int_0^L Y_0(x) (\delta\lambda(x, 0)) dx - \int_0^T Y_l(t) (\delta\gamma(0, t)) dt = 0; \quad (22) \\
 & \delta\lambda(x, T) = 0; \quad \delta\gamma(L, t) = 0; \\
 & \lambda(x, T) = \lambda_T(T); \quad \gamma(L, t) = \gamma_r(t),
 \end{aligned}$$

where  $\lambda_T(\cdot)$  and  $\gamma_r(\cdot)$  are arbitrarily specified functions.

## 4 Algorithm

As introduced in [1], we compute approximate solutions to the problems of interest by solving them in a time-concatenated series of space-time subdomains whose (closed) union forms (the closure of) the entire domain  $\Omega$  of interest. We solve a distinct, dual (space-time) bvp in each of these stages, step-by-step, marching in time, where the initial condition and base state in any stage depends on the output produced from the previous stage, details of which will be explained in the description of example problems to follow. Each of these subdomains,  $\Omega^{(s)}$ , is referred to as a *stage*, indexed by  $s = 1, 2, 3, \dots, N$ ,  $\bar{\Omega} = \cup_{s=1}^n \bar{\Omega}^{(s)}$ .

A two-point Gauss quadrature scheme, in each of the  $x$  and  $t$  directions, has been utilized to approximate all the domain and boundary integrals appearing in the work. We will refer to the collection of nodes corresponding to a specific time (falling on the nodes of discretization) as a *nodal timeline*. Similarly, we will refer to the collection of all Gauss points corresponding to a particular time as a *Gauss timeline*. The setup for a sample mesh of  $2 \times 2$  has been shown in Fig. 2a.

Due to the nature of the arbitrarily chosen (without loss of generality) 0 b.c. utilized on the dual fields ((4) and (17)) at the final-time boundary of a stage, strong gradients/boundary-layers can arise in the dual solution that can require excessive refinement to resolve. Since the time-like extent of any stage is an arbitrary choice subject only to computational expediency and accuracy, in every stage, solutions obtained for a specified layer of elements in the time-like direction near the final time boundary of the stage are ignored. We refer to this operation as ‘truncation’. The following stage initiates from a suitable time near the end of the current stage on the retained mesh (either at a Gauss timeline or at a nodal timeline, see Fig. 2a), referred to as the ‘cutoff’ line. A visual representation illustrating this concept is presented in the Fig. 2c.

We employ the Newton Raphson method (NR) within each stage to approximate the solutions. A linear span of globally continuous, piecewise smooth finite element shape functions corresponding to an FE mesh for  $\Omega^{(s)}$  is used to achieve this discretization. These shape functions are represented by  $N^{(\cdot)}$ , where  $(\cdot)$  denotes the index of any node on the space-time mesh. Let  $D$  and  $U$  represent the set of dual and primal variables for the problem under consideration. So, for the Burgers equation,

$$D := (D_1) = (\lambda); \quad U := (U_1) = (u),$$



whereas for the Burgers-HJ,

$$D := (D_1, D_2) = (\lambda, \gamma); \quad U := (U_1, U_2) = (Y, u).$$

The discretized dual fields and test functions are expressed as

$$D_i(x, t) = D_i^A N^A(x, t); \quad \delta D_i(x, t) = \delta D_i^A N^A(x, t); \quad dD_i(x, t) = dD_i^A N^A(x, t), \quad (23)$$

where  $D_i^A$  denotes the finite element nodal degrees of freedom. The discretized version of the appropriate weak form (11) or (22) generates a discrete residual  $R_i^A(\mathcal{D})$  (derived in Sec. 5.1 for the Burgers equation and Sec. 5.2 for the Burgers-HJ) given by

$$R[D; \delta D] = \delta D_i^A R_i^A(\mathcal{D})$$

and its variation in the direction  $dD$ , the Jacobian

$$J[D; \delta D, dD] = \delta D_i^A J_{ij}^{AB}(\mathcal{D}) dD_j^B.$$

Any stage begins with an initial guess of  $D_i^{A(0)} = 0$  followed by solving the following matrix equation for the  $k^{th}$  correction:

$$\begin{aligned} -R_i^A(\mathcal{D}^{(k-1)}) &= J_{ij}^{AB}(\mathcal{D}^{(k-1)}) dD_j^B \\ D_j^{B(k)} &= D_j^{B(k-1)} + dD_j^B, \end{aligned} \quad (24)$$

where  $\mathcal{D} = (\partial_t \lambda, \partial_x \lambda)$  for the Burgers equation and  $\mathcal{D} = (\lambda, \gamma, \partial_t \lambda, \partial_x \gamma)$  for Burgers-HJ. The convergence criteria for NR is set as follows:

$$\max_{A,i} |R_i^A| < tol,$$

where  $tol$  represents a user-defined threshold tolerance.

The following notation is used in the algorithm:

$(\cdot)^{(s)(k)}$	value of $(\cdot)$ at $k^{th}$ NR iterate for stage $s$
$N_x$	number of elements in $x$ direction
$N_t^{(s)}$	number of elements in $t$ direction per stage
$t_i^{(s)}$	time at the start of stage $s$
$T^{(s)}$	time over which the stage $s$ is solved
$t_f^{(s)}$	time at the cutoff line for stage $s$
$\Omega^{(s)}$	$(0, L) \times (t_i^{(s)}, t_i^{(s)} + T^{(s)})$ ; domain for stage $s$
$\bar{U}_k^{(s)}$	base state for $U_k$ in stage $s$
$\beta_k$	coefficient(s) defining $H$ in (6) or (15)
$U_0^{(s)}$	primal initial condition for stage $s$
$\Omega^{(s)\times}$	discarded domain for the stage $s$
$N_c \times N_x$	number of discarded elements per stage

The algorithm has been presented in table 1. Additional details for the algorithm are as follows:

---

**Algorithm**

---

**Initialization:**

1. Set  $s = 1$ ,  $t_f^{(0)} = 0$  and  $U_0^{(1)}(x)$  from (3) or (14) depending on the problem under consideration.
  2. Choose the values for  $T^{(s)}$ ,  $N_x$ ,  $N_t^{(s)}$ ,  $\beta_k$ ,  $N_c$  and  $tol$ .
- 

 **$s$ th stage:**

1. Set  $t_i^{(s)} = t_f^{(s-1)}$  and generate  $U_0^{(s)}$  ( $s > 1$ , see Sec. 5 for details). Over the domain  $\Omega^{(s)}$ , set appropriate  $\bar{U}_k^{(s)}$ .
  2. Initiate NR: Set  $D_k^{A(s)(0)} = 0$ .  
**For**  $j \geq 0$ :
    - i Evaluate  $R_i^{A(s)(j)}$ .
    - ii Set  $d^{(s)(j)} = \max_{A,i} |R_i^{A(s)(j)}|$ .  
**if**  $d^{(s)(j)} < tol$  **then** go to step 3 (exit loop).  
**else** continue.
    - iii Evaluate  $J_{ij}^{AB(s)(j)}$ .
    - iv Evaluate  $D_k^{A(s)(j+1)}$  using (24).
    - v **do**  $j = j + 1$  and **go to** step 2i
  3.  $D_k^{(s)(j)}$  serves as the dual solution for the current stage, while the corresponding  $U_k$  serves as the solution for the primal problem. Discard the results obtained in the region  $\Omega^{(s)\times}$ .
  4. Set an appropriate  $t_f^{(s)}$  near the final time obtained on  $\Omega^{(s)} \setminus \Omega^{(s)\times}$ .
  5. Set  $s = s + 1$  and repeat steps 1-4 until  $t_f^{(s)} \geq T$
- 

**Table 1:** Algorithm to solve Burgers equation or Burgers-HJ. The subscript index  $k$  takes the value of 1 for Burgers and ranges over (1, 2) for Burgers-HJ.

- Corresponding to the discretized dual fields  $D$ , the primal field  $U$  can be evaluated using the appropriate DtP mapping (7) or (16) on the Gauss points within any element, which is further used in the evaluation of  $R_i^A$  and  $J_{ij}^{AB}$ .
- For each stage, we discard the results over the final  $T_c$  duration of time in that stage (see Fig. 2c). Denoting by  $T_e$  the edge-length of elements in the time-like direction (see Fig. 2a), the truncation operation is carried out over  $N_c := \frac{T_c}{T_e}$  space-like layers of elements.
- For the Burgers equation,  $U_0(x) := u_0(x)$ , whereas for the Burgers-HJ,  $U_0(x) := Y_0(x)$ . For the first stage, initial condition is used from the problem definition (3) or (14), and for all subsequent stages, the initial condition is generated from the output of the previous stage (see Sec. 4.1 and Sec. 4.2). The primal boundary conditions obviously need no adjustment in the course of dual time evolution. These initial and boundary conditions enter into the dual formulation as natural boundary conditions in each stage.

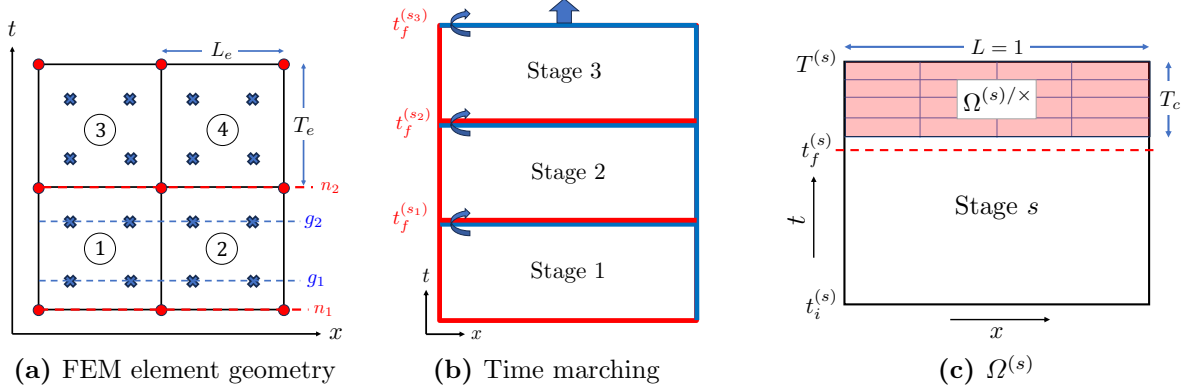


**Figure 2:** (a) A sample  $2 \times 2$  mesh with element numbers at center. Red dashed lines, passing through the nodal points (red dots), represent nodal timelines.  $g_1$  and  $g_2$  represent the first and the second Gauss timelines passing through the Gauss points of the elements 1 and 2. (b) represents the concatenated domains after truncation. Additionally,  $t_f^{(s)} = t_i^{(s+1)}$ .

- To evaluate the quality of the results produced via the algorithm, the corresponding exact entropy solution to each example is presented in Appendix E.

The figures presented in this work are produced as follows: For each Gauss timeline, we compute the average of the primal data obtained from the two Gauss points within each element through which the Gauss timeline traverses. This average is then assigned to the  $x$ -coordinate of the element center and  $t$ -coordinate of the Gauss timeline under consideration.

We demonstrate and discuss the results of the computation of five selected examples that are used to evaluate and understand our dual scheme applied to the Burgers equation and its corresponding Hamilton-Jacobi form. Sec. 5.1 and Sec. 5.2 deal with the inviscid case of the Burgers equation and Burgers-HJ, respectively, and we often omit the adjective ‘inviscid.’ Specific details related to each of these equations are presented below.

#### 4.1 Algorithmic details for the Burgers equation

In order to evaluate solutions to the dual form of the Burgers equation (10), we utilize the residual (11) and generate the corresponding Jacobian by considering its variation in a direction  $d\lambda$ :

$$J[\delta\lambda; d\lambda] = \int_{\Omega} \left( -\partial_t \delta\lambda \left( \frac{\partial \hat{u}}{\partial \mathcal{D}_i} d\mathcal{D}_i \right) - \hat{u} \partial_x \delta\lambda \left( \frac{\partial \hat{u}}{\partial \mathcal{D}_i} d\mathcal{D}_i \right) \right) dt dx,$$

where  $\mathcal{D} := (\partial_t \lambda, \partial_x \lambda)$ .

We employ the approximate dual field (23) in the residual (11) to generate a discrete residual  $R^A$  at each node  $A$  given by

$$R^A = \int_{\Omega} \left( -\hat{u} \partial_t N^A - \frac{\hat{u}^2 \partial_x N^A}{2} \right) dt dx - \int_0^L u_0(x) N^A(x, 0) dx - \int_0^T u_l(t) N^A(0, t) dt.$$

However,  $R^A = 0$  is not imposed for all the nodes corresponding to the right and top boundaries as a consequence of the Dirichlet b.cs (4). The discrete Jacobian matrix associated with the pair

of degrees of freedom  $(A, B)$  (the coefficient of the term  $(\delta\lambda^A d\lambda^B)$ ) is given by

$$J^{AB} = \int_{\Omega} \left( -\partial_t N^A - \hat{u} \partial_x N^A \right) \left( \frac{\partial \hat{u}}{\partial \mathcal{D}_i} \partial_i N^B \right) dt dx;$$

$$\frac{\partial \hat{u}}{\partial(\partial_t \lambda)} = \frac{1}{\beta_u - \partial_x \lambda}; \quad \frac{\partial \hat{u}}{\partial(\partial_x \lambda)} = \frac{\hat{u}}{\beta_u - \partial_x \lambda},$$

where  $\partial_1(\cdot) = \partial_t(\cdot)$  and  $\partial_2(\cdot) = \partial_x(\cdot)$ .

Based on the algorithm presented in Table. 1, after truncation, the cutoff line for each stage (from which the next stage commences) is the  $g_2$  Gauss timeline of the last layer of retained elements with  $t_f^{(s)}$  the corresponding physical time. The data for  $\hat{u}$  obtained at this time (required only at Gauss points) is denoted by  $\hat{u}^{(s)}(x, t_f^{(s)})$ . The initial condition and the base state for the next stage is set as

$$u_0^{(s+1)}(x) = \hat{u}^{(s)}(x, t_f^{(s)});$$

$$\bar{u}^{(s+1)}(x, t) = \mathcal{S} \left[ \hat{u}^{(s)}(x, t_f^{(s)}) \right],$$

where  $\mathcal{S}$  denotes a smoothing operator, and the specific details can be found in Appendix D. In essence, the primal fields generated in each stage, relying on the dual fields and their derivatives, may exhibit oscillations, particularly in the vicinity of any shock; the smoothing operation mitigates these high-wave number oscillations in the base state for the subsequent stage that remains constant throughout the subsequent cycle. *We note that such smoothing is not used to define the initial condition for the next stage.*

## 4.2 Algorithmic details for the Burgers-HJ

To assess solutions to (20), we employ the residual (22) and generate a corresponding Jacobian by considering its variation in the direction  $dD := (d\lambda, d\gamma)$ , expressed as

$$J[\delta\lambda, \delta\gamma; d\lambda, d\gamma] = \int_{\Omega} \left( (-\partial_t(\delta\lambda) - \partial_x(\delta\gamma)) \left( \frac{\partial \hat{Y}}{\partial \mathcal{D}_i} d\mathcal{D}_i \right) + (\hat{u} \delta\lambda - \delta\gamma) \left( \frac{\partial \hat{u}}{\partial \mathcal{D}_i} d\mathcal{D}_i \right) \right) dt dx, \quad (25)$$

where  $\mathcal{D} := (\partial_t \lambda, \partial_x \gamma, \lambda, \gamma)$ . The discrete version for the residual (22), computed using the approximate dual fields  $D$  as defined in (23), for each node  $A$  is given by

$$R_1^A = \int_{\Omega} \left( -\hat{Y} \partial_t N^A + \frac{\hat{u}^2 N^A}{2} \right) dt dx - \int_0^L Y_0(x) (N^A(x, 0)) dx;$$

$$R_2^A = \int_{\Omega} (-\hat{Y} \partial_x N^A + \hat{u} N^A) dt dx - \int_0^T Y_l(t) (N^A(0, t)) dt.$$

$R_1^A = 0$  for all the nodes corresponding to the top boundary and  $R_2^A = 0$  for all the nodes corresponding to the right boundary are not imposed as a consequence of the Dirichlet b.cs (17). The discrete version of the Jacobian corresponding to the degree of freedom pair  $(A, i), (B, j)$  is

given as follows:

$$\begin{aligned}
J_{11}^{AB} &= \int_{\Omega} \left( -\frac{\partial \hat{Y}}{\partial(\partial_t \lambda)} \partial_t N^A \partial_t N^B + \hat{u} \frac{\partial \hat{u}}{\partial \lambda} N^A N^B \right) dt dx; \\
J_{12}^{AB} &= \int_{\Omega} \left( -\frac{\partial \hat{Y}}{\partial(\partial_x \gamma)} \partial_t N^A \partial_x N^B + \hat{u} \frac{\partial \hat{u}}{\partial \gamma} N^A N^B \right) dt dx; \\
J_{21}^{AB} &= \int_{\Omega} \left( -\frac{\partial \hat{Y}}{\partial(\partial_t \lambda)} \partial_x N^A \partial_t N^B - \frac{\partial \hat{u}}{\partial \lambda} N^A N^B \right) dt dx; \\
J_{22}^{AB} &= \int_{\Omega} \left( -\frac{\partial \hat{Y}}{\partial(\partial_x \gamma)} \partial_x N^A \partial_x N^B - \frac{\partial \hat{u}}{\partial \gamma} N^A N^B \right) dt dx; \\
\frac{\partial \hat{Y}}{\partial(\partial_t \lambda)} &= \frac{1}{\beta_Y}; & \frac{\partial \hat{Y}}{\partial(\partial_x \gamma)} &= \frac{1}{\beta_Y}; \\
\frac{\partial \hat{u}}{\partial \lambda} &= -\frac{\hat{u}}{\beta_u + \lambda}; & \frac{\partial \hat{u}}{\partial \gamma} &= \frac{1}{\beta_u + \lambda}.
\end{aligned}$$

In contrast to the examples associated with the Burgers equation, the oscillations observed in the solution (for  $\hat{Y}$  here) obtained on the Gauss points are significantly more pronounced. To address this issue, in each stage, the truncation is followed by an  $L^2$  projection of  $\hat{Y}$  (Appendix. C) along the  $n_2$  nodal timeline of the last layer of elements obtained on the retained mesh. Such an operation provides us with a continuous  $C^0$  approximant along the considered nodal timeline. This timeline also serves as the cutoff line for the current stage. The initial condition and the base states for the following stage are set as follows:

$$\begin{aligned}
Y_0^{(s+1)}(x) &= L^2 \left[ Y^{(s)} \left( x, t_f^{(s)} \right) \right]; \\
\bar{Y}^{(s+1)}(x, t) &= Y^{(s)} \left( x, t_f^{(s)} \right); & \bar{u}^{(s+1)} &= \frac{d}{dx} Y^{(s)} \left( x, t_f^{(s)} \right),
\end{aligned}$$

where  $L^2[\cdot]$  represents the  $L^2$  projection operator. Unlike the scheme for the Burgers equation, no smoothing for base states is used for the inviscid Burgers-HJ algorithm.

## 5 Results

To evaluate the dual scheme, we demonstrate five examples for the two types of equations, each presenting distinct levels of complexity. For each of the examples introduced in Sec. 5.1, a related example is generated in Sec. 5.2. This associated example is supplied with the initial and boundary conditions in a manner that the exact entropy solution produced by the Burgers-HJ equation should have its derivative equal to the exact entropy solution obtained for the corresponding problem from the Burgers equation.

### 5.1 Burgers Equation

For each of the examples presented in this section, the following parameters were set for each stage in the algorithm:  $T^{(s)} = 5 \times 10^{-3}$ ,  $N_x = 100$ ,  $N_t^{(s)} = 100$ ,  $\beta_k = 10^6$ ,  $N_c = 5$  and  $tol = 10^{-16}$ . This amounts to a fairly fine discretization of the problem, but our main goal here is not to probe the computational efficiency of the proposed elementary scheme, but to simply use it to evaluate and understand the capabilities of our dual variational formulation for nonlinear PDE in this specific context.

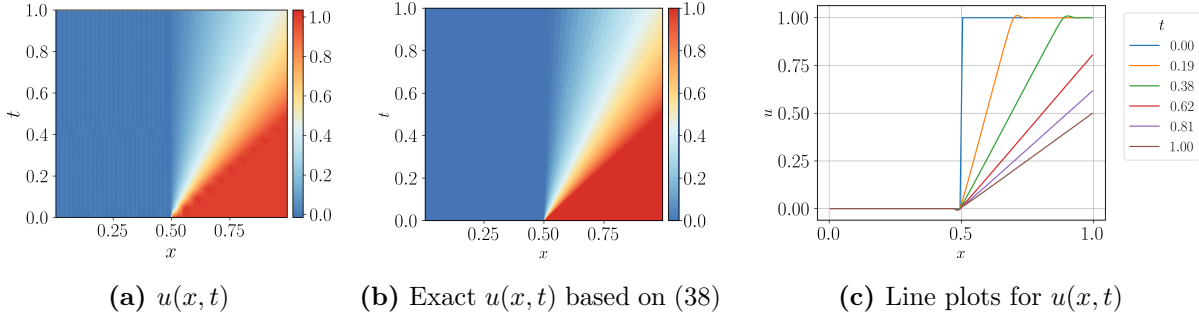


**Figure 3:** DtP mapping generated primal field  $u$  for the expansion fan. Fig. (c) shows minor overshoots as the fan opens up which may be attributed to the  $C^0$  approximation of the dual fields.

### 5.1.1 Expansion Fan

We consider the Riemann problem corresponding to an expansion fan solution with initial condition given by:

$$u_0(x) = \begin{cases} U_L = 0 & \text{for } x < 0.5 \\ U_R = 1 & \text{for } x > 0.5. \end{cases} \quad (26)$$

The problem has non-unique weak solutions (consisting of the continuous rarefaction wave and an entire family of discontinuous solutions with shocks), and a unique ‘entropy’ solution is obtained by imposing an entropy condition [9, 10] (also see App. E). This entropy solution is a rarefaction wave, which for  $t > 0$  in an infinite domain is given by (38).

We use the primal boundary condition  $u_l(t) = 0$  and apply the Dirichlet b.cs  $\lambda_T(x) = \lambda_r(t) = 0$ . The results for this setup are shown in Fig. 3.

Comparing Fig. 3a against Fig. 3b, it is surprising to see that the dual scheme automatically picks up only the entropy solution without enforcing any further conditions, and seems to be incapable of recovering the other possible weak solutions for the equation.

### 5.1.2 Shock

We next consider the Riemann problem (26) with

$$U_L = 1; \quad U_R = 0.$$

The exact entropy solution to this problem on an infinite domain is given by (40).

We use the primal boundary condition  $u_l(t) = 1$  and apply the Dirichlet b.cs  $\lambda_T(x) = \lambda_r(t) = 0$ . The results for this setup has been shown in Fig. 4. The over(under)shoot seen around the shock profile at any time in Fig. 4b arise due to the  $C^0$  FE interpolation of the dual fields. Nevertheless, the shock profile effectively captures the accurate height and speed, aligning closely with the exact entropy solution.

### 5.1.3 Double Shock

Here we assess the dual formulation in the setting of two traveling shocks interacting with each other. Consider the following initial condition

$$u_0(x) = \begin{cases} 1 & \text{for } x < 0.25 \\ 0.5 & \text{for } 0.25 < x < 0.5 \\ 0 & \text{for } x > 0.5. \end{cases}$$

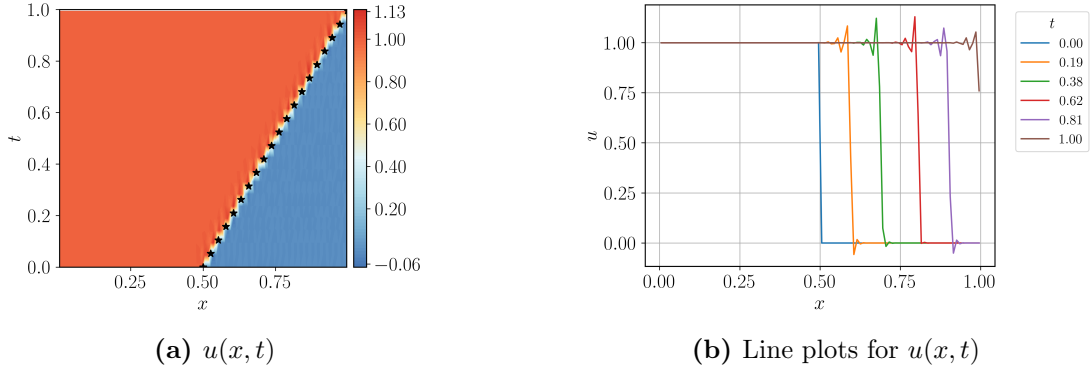


**Figure 4:** DtP mapping generated primal field  $u$  for the shock problem. In Figure (a), the black asterisks represent the shock trajectory based on the exact entropy solution, which is being superimposed on the original plot.

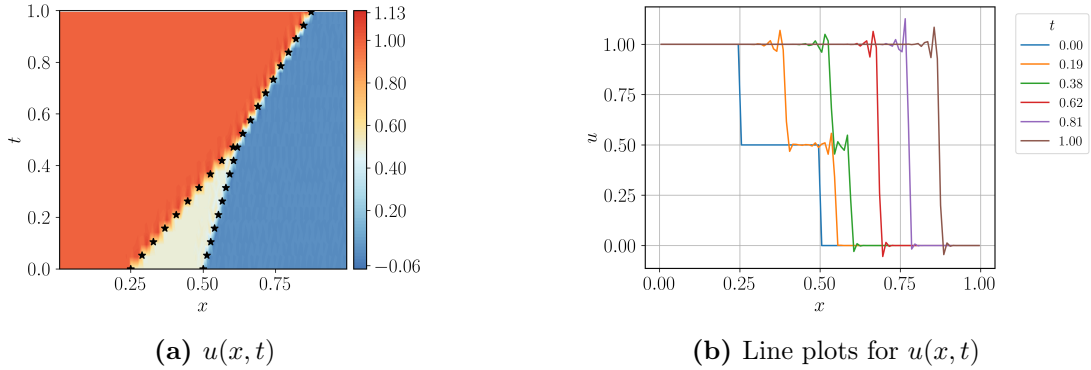


**Figure 5:** DtP mapping generated primal field  $u$  for a double shock. In Figure (a), the black asterisks represent the shock trajectories for the two shocks based on the exact entropy solution, which is being superimposed on the original plot. The two shocks merge at  $(x, t) = (0.625, 0.5)$

The solution to this problem on an infinite domain is given by (42).

We use the primal boundary condition  $u_l(t) = 1$  and apply the Dirichlet b.cs  $\lambda_T(x) = \lambda_r(t) = 0$ . The results for this setup are shown in Fig. 5.

Evident from Fig. 5b, the instabilities near the two shocks, caused by the continuous interpolation, do not accumulate as the shocks merge. Instead, they vanish, leaving no indication of a double shock presence. Based on Fig. 5a, it is also evident that the dual problem correctly captures the accurate shock speeds for each individual shock.

#### 5.1.4 Half N-wave

The objective of this problem is to evaluate the dual formulation when a shock wave decreases in size and experiences a change in speed during its propagation Fig. E.4. We call this problem as a *half N-wave*, adapting standard terminology in the literature (even though it looks like a ‘reflected’ half  $N$ ). Consider the following initial condition:

$$u_0(x) = \begin{cases} 0 & \text{for } x < x_0 \\ \frac{h_0}{l_0}(x - x_0) & \text{for } x_0 \leq x < x_0 + l_0 \\ 0 & \text{for } x > x_0 + l_0, \end{cases}$$

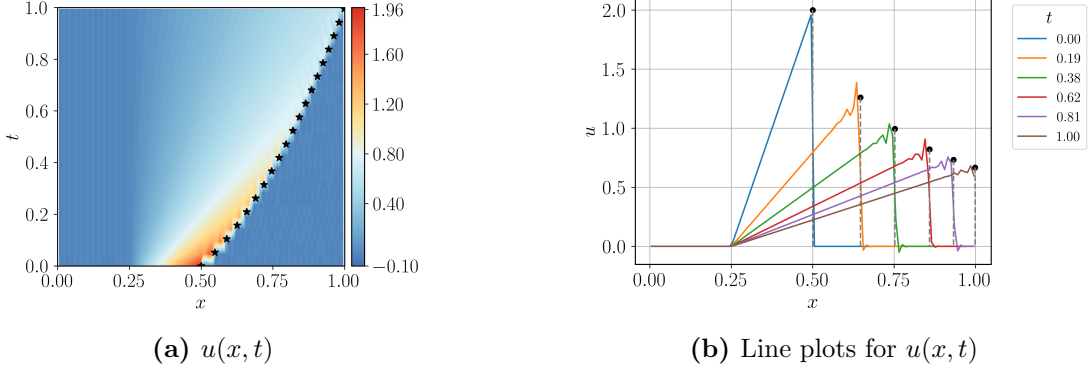


**Figure 6:** DtP mapping generated primal field  $u$  for the half N-wave problem. In Fig.(a), the black asterisks represent the shock trajectory based on the exact entropy solution, which is being superimposed on the original plot. In Figure (b), the adjacent black lines, aligned with the original plot lines at various time points, depict the position and height of the shock based on the exact entropy solution for those respective times.

where  $x_0 = 0.25$ ,  $l_0 = 0.25$  and  $h_0 = 2$ . The solution to this problem on an infinite domain is given by (44).

We use the primal boundary condition  $u_l(t) = 0$  and apply the Dirichlet b.cs  $\lambda_T(x) = \lambda_r(t) = 0$ . The results for this setup are shown in Fig. 6.

The geometry in this example is more intricate compared to previous examples, featuring both a fan at  $x = 0.25$  and a traveling shock. As explained in Appendix. E.4, conservation of the area under the right-angled triangle dictates the speed and the height of the shock, which vary non-linearly in time. The dual formulation successfully captures this phenomenon.

### 5.1.5 N-wave

The objective of this problem is to evaluate the dual formulation in the context of two expansion fans in opposite directions converging to form a standing shock whose magnitude dissipates over time (Fig. 19a). Consider the following initial condition:

$$u_0(x) = \begin{cases} 0 & \text{for } x < 0.25 \\ -4h_0(x - 0.5) & \text{for } 0.25 \leq x < 0.75 \\ 0 & \text{for } x > 0.75; \end{cases}$$

$$h_0 = 2.$$

The solution to this problem on an infinite domain is given by (48).

We use the primal boundary condition  $u_l(t) = 0$  and apply the Dirichlet b.cs  $\lambda_T(x) = \lambda_r(t) = 0$ .

Based on the discussion found in E.5 related to Fig. 19b, each of the two tips at  $x = 0.25$  and  $x = 0.75$  travel in opposite directions while maintaining a constant speed and height. The information originating from the range  $x \in (0.25, 0.75)$  at time  $t = 0$  ultimately converges to form a standing shock at  $x = 0.5$  and  $t_m = 0.125$ . Subsequently, the standing shock gradually self-annihilates. The results based on the dual scheme for this setup, shown in Fig. 7, manages to capture this whole sequence of events quite well.



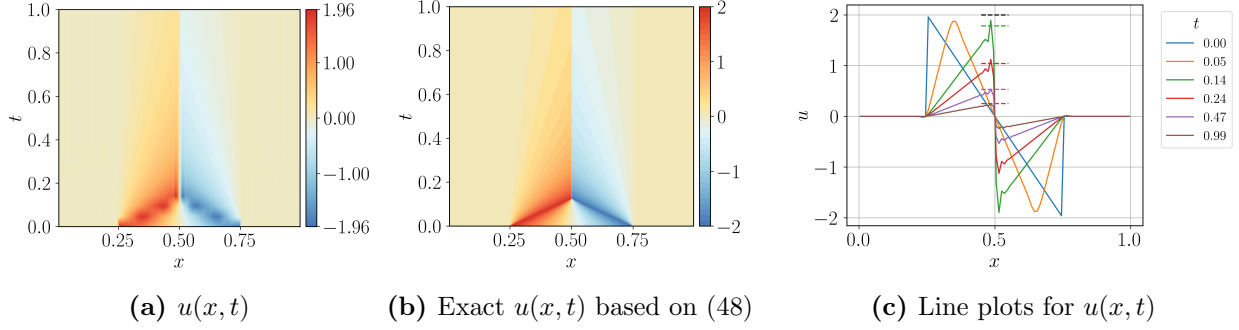


**Figure 7:** DtP mapping generated primal field  $u$  for the N-wave problem. In Fig. 7c, the dashed lines use colors matching those of the line plots at specific times to represent the true height at those times according to the exact entropy solution. The black dashed line corresponds to the height of the tip before the shock formation occurs.

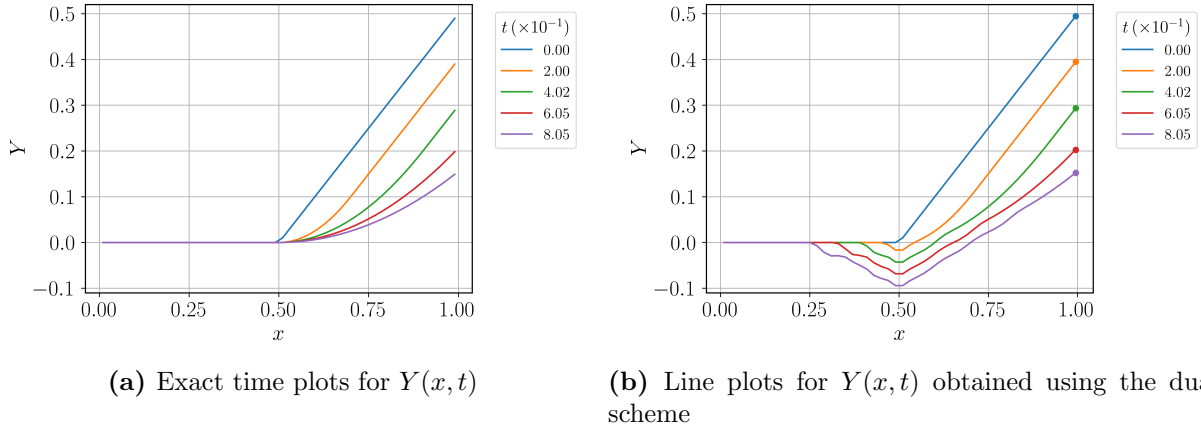


**Figure 8:** The two plots have been drawn on same scale. Fig.(b) shows DtP mapping generated primal field  $Y$  for the Fan problem. The dots in various colors at  $x = 1$  correspond to the exact value of  $Y$  derived from the exact entropy solution (39), corresponding to the time indicated by the color of each respective dot.

## 5.2 Inviscid Burgers-HJ

For the examples presented in this section, the following parameters were set for each stage in the algorithm:  $\beta_Y = \beta_u = 10^6$ ,  $N_c = 5$  and  $tol = 10^{-16}$ . The parameters defining the mesh were  $N_x = 50$ ,  $N_t^{(s)} = 10$  with  $T^{(s)} = 5 \times 10^{-3}$ . This is again a fine discretization, and our concern here is simply to evaluate the dual formulation of the problem.

### 5.2.1 Expansion Fan

Consider the following initial condition:

$$Y_0(x) = \begin{cases} 0 & \text{for } x < 0.5 \\ x & \text{for } x > 0.5. \end{cases}$$

The exact entropy solution for this setup on an infinite domain is given by (39). To evaluate the dual solutions numerically on  $\Omega$ , we impose  $Y_l(t) = 0$ , naturally. The results obtained for this setup are show in Fig. 8, which shows an unexpected dip in the  $Y$  profiles at  $x = 0.5$ .

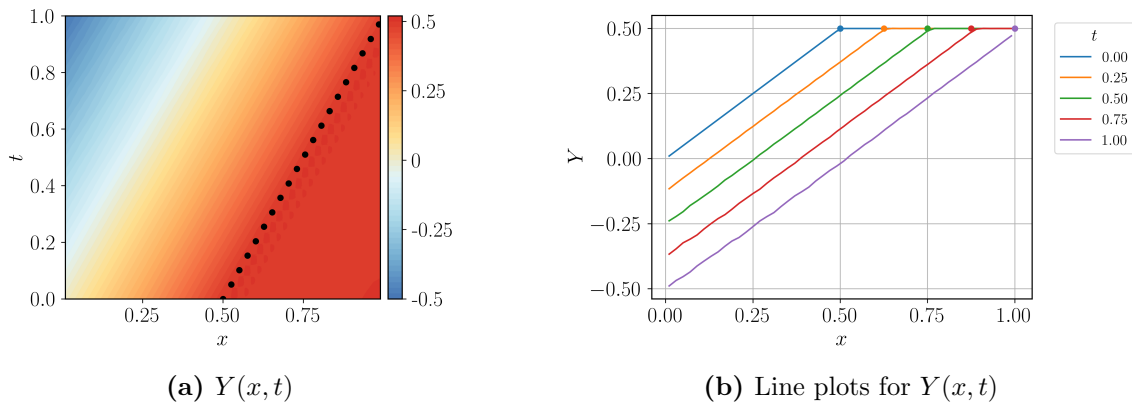


**Figure 9:** DtP mapping generated primal field  $Y$  for the Shock problem. In Figure(a), the black dots represent the trajectory of the kink based on the exact entropy solution (41). In Figure (b), the dots plotted at  $Y = 0.5$  with colors matching those of the line plots represent the position of the kink based on the exact  $Y$  profile (41) at that specific time.

This discrepancy indicates that the dual scheme does not capture the entropy solution for this particular setup. Upon closer inspection one can notice that the dip actually represents a standing shock which can be confirmed by approximating the spatial gradient ( $u$ ) to the immediate left and to the right of  $x = 0.5$ , and using the Rankine-Hugoniot jump condition such that

$$c(x = 0.5, t) = \frac{\partial_x Y(x = 0.5^+, t) + \partial_x Y(x = 0.5^-, t)}{2} \approx \frac{1 + (-1)}{2} = 0.$$

Thus the evolution profiles indicates that a fan breaks up into a locally standing shock which then propagates information in both directions. We note that within an expansion fan, a shock is acceptable as a weak solution.

### 5.2.2 Shock

Consider the initial condition and the boundary condition given by

$$Y_0(x) = \begin{cases} x & \text{for } x < 0.5 \\ 0.5 & \text{for } x > 0.5; \end{cases}$$

$$Y_l(t) = -\frac{t}{2},$$

respectively. For these conditions, we expect to recover the solution given by (41), the derivative of which recovers the shock presented in 5.1.2. The  $Y$  data obtained at different times from the simulation of the dual problem has been shown in Fig. 9.

Referring to Fig. 9b, it is apparent that kink in the  $Y$  profiles moves at an approximate speed of 0.5. This kink signifies the presence of a shock in the  $u$  profile, where the slope of the  $Y$  (equivalent to  $u$ ) profile changes from 1 to 0. As depicted in Fig. 9b, minor oscillation-type instabilities are still noticeable in the  $Y$  profiles as time advances.

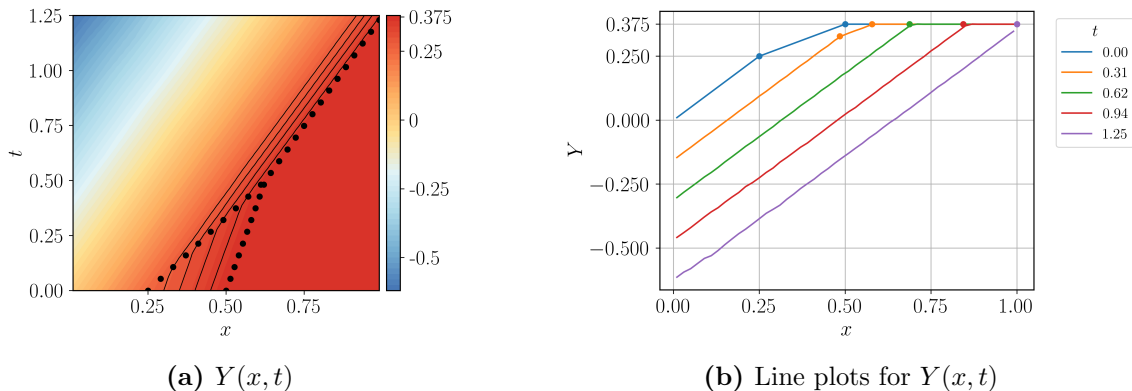


**Figure 10:** DtP mapping generated primal field  $Y$  for the double shock. In Fig.(a), the black dots represent the trajectory of the two kinks in the space-time domain based on the exact expressions (43). The solid black lines represent contour lines corresponding to the characteristics of  $u$  derived through dual scheme in the vicinity of the double shock. In Figure (b), the dots plotted with colors matching those of the line plots represent the position and height of the kinks based on the exact  $Y$  profile (43) at that specific time.

### 5.2.3 Double Shock

Consider the initial condition and the boundary condition given by

$$Y_0(x) = \begin{cases} x & \text{for } x < 0.25 \\ x/2 + 0.125 & \text{for } 0.25 < x < 0.5 \\ 0.375 & \text{for } x > 0.5; \end{cases}$$

$$Y_l(t) = -\frac{t}{2},$$

respectively. For these conditions, we expect to recover the solution given by (43), the derivative of which recovers the double shock presented in 5.1.3. The results for this setup are shown in Fig. 10.

Similar to the shock example, this problem has two kinks emanating at  $t = 0$  corresponding to the two shocks, traveling at different speeds, merging at  $t = 0.5$ . Apparent from Fig. 10a, the characteristics originating between  $x = 0.25$  and  $x = 0.5$  move at a slower speed compared to the approaching kink from the left, eventually merging with it. The dual formulation captures this phenomenon, although (very minor) instabilities are again visible as evident in Fig. 10b

### 5.2.4 Half N-wave

Consider the following equation set:

$$Y_0(x) = \begin{cases} 0 & \text{for } x < x_0 \\ \frac{h_0}{l_0} \left( \frac{x^2 + x_0^2}{2} - x_0 x \right) & \text{for } x_0 \leq x < x_0 + l(t) \\ \frac{h_0 l_0}{2} & \text{for } x > x_0 + l(t). \end{cases}$$

The exact expression for  $Y$  for this setup is given by (45), the spatial derivative of which represents the Half N-wave presented in Sec. 5.1.4. The results obtained via our dual scheme is shown in Fig. 11.

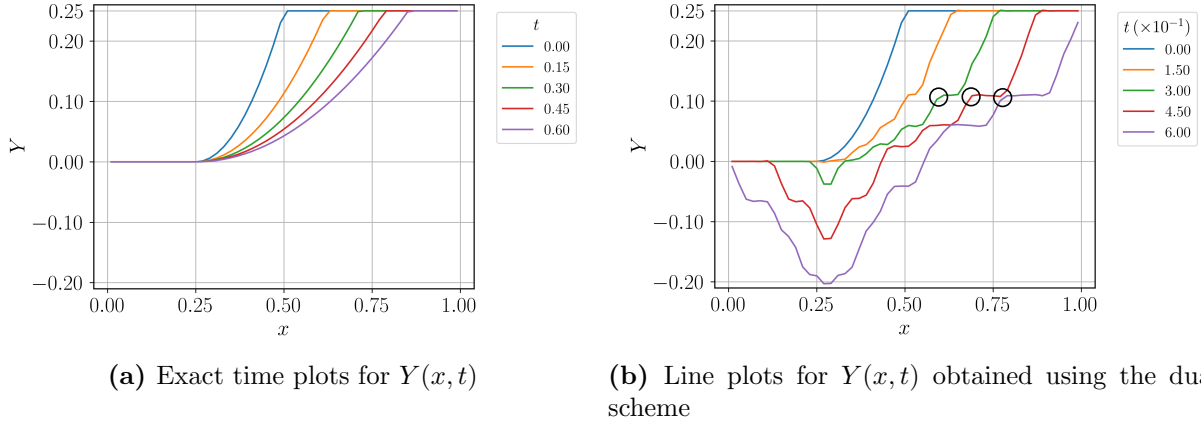


**Figure 11:** The two plots have been drawn on same scale. Fig.(b) represents the DtP mapping generated  $Y$  profiles. The black circles along the kinks represent the trajectory of one of the multiple kinks whose spatial derivatives exhibit a shock-like behavior.

Comparing against the profiles for  $Y$  based on the exact entropy solution illustrated in 11a, we immediately notice the standing shock behavior (as in the case of the fan example) here at  $x = 0.25$ . Additionally, we notice several small shock-like structures nucleating one after other at different points in space as the curved section of the profile between  $x = 0.25$  and  $x = 0.5$  advances. A ‘shock’ speed analysis similar to the fan example, but now on one such structure characterized by a kink for which the spatial derivative ( $u$ ) approximately goes from 1 to 0 (shown by the circles in Fig. 11b), reveals that the distance travelled by this kink in a given time approximates well the distance suggested by the ‘shock speed’ of the kink within that time, establishing that these structures indeed behave like shocks.

### 5.2.5 N-wave

As the last example, the following initial and boundary conditions are considered:

$$Y_0(x) = \begin{cases} 0 & \text{for } x < 0.25 \\ -2h_0(x^2 - x) - 3h_0/8 & \text{for } 0.25 \leq x < 0.75 \\ 0 & \text{for } x > 0.75; \end{cases}$$

$$Y_l(t) = 0;$$

$$h_0 = 2.$$

The exact entropy solution for this setup is given by (49), which gets approximated well based on the profiles displayed in Fig. 12, although we again notice the standing shock formations at  $x = 0.25$  and  $x = 0.75$  after a certain time based on Fig. 12b.

## 5.3 Viscous Burgers-HJ

Evident from the examples presented in the last section, the dual scheme does not recover the entropy solutions in the case of the Fan 5.2.1, the Half N-wave 5.2.4 and the N-wave 5.2.5. As mentioned previously, for any Riemann problem of the form (26) with  $U_R > U_L$ , the equation has non-unique weak solutions and the entropy condition, i.e. information along characteristics travel towards the shock-curve in space-time and not away from it, acts to select a solution, in this case a

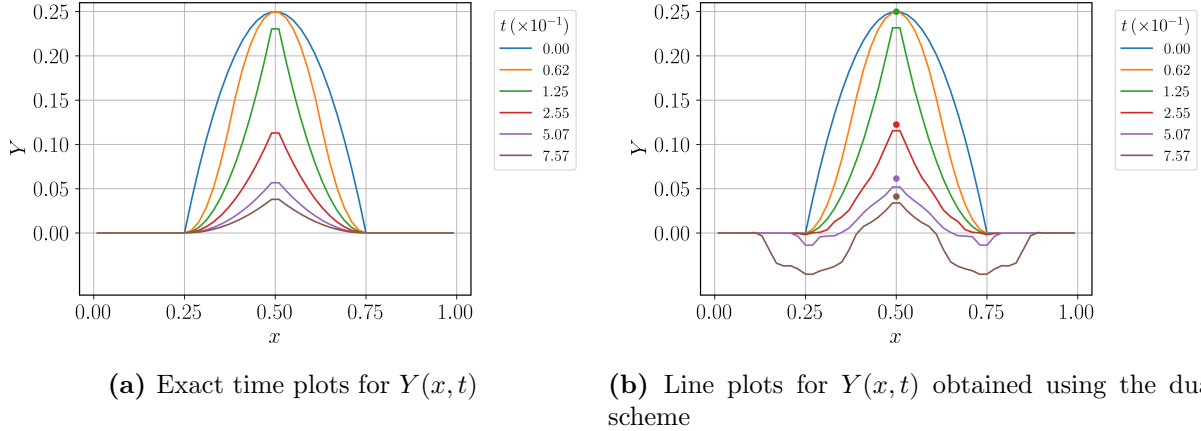


**Figure 12:** The two plots have been drawn on same scale. Fig.(b) represents the DtP mapping generated  $Y$  profiles. The dots in various colors at  $x = 0.5$  correspond to the exact value of  $Y$  derived from (49), corresponding to the time indicated by the color of each respective dot, after the kink formation takes place at  $t = 0.125$ .

fan. This ambiguity disappears when viscosity is introduced; indeed, entropy solutions for inviscid Burgers(-HJ) are known to be limits of Burgers solutions as  $\nu \rightarrow 0$ . While our scheme recovers entropy solutions when dealing with the Burgers equation examples in Sec. 5.1, this does not happen with the computational scheme for Burgers-HJ, and it appears to recover a greater variety of weak solutions (which, in a sense, is what the scheme, in and of itself, is required to do without any further conditions). The examples presented in the last section demonstrate this point.

Considering the functional (19), it is evident that the derivative  $\partial_x \lambda$  is not being penalized. This allows for spatial discontinuities to exist in  $\lambda$  (that may arise from even inevitable numerical round-off errors in  $\lambda$ ), and correspondingly in  $\hat{u}$  due to the DtP mapping (16b). These discontinuous will be propagated in the spatial domain due to the inherent characteristics of the inviscid Burgers equation. To test this hypothesis, we work with a dual formulation of Burgers-HJ (12) with  $\nu \neq 0$ .

The first order system associated with (12) can be written as

$$\partial_t Y = -\frac{u^2}{2} + \nu \partial_x u \quad \text{in } \Omega; \quad (27a)$$

$$\partial_x Y = u \quad \text{in } \Omega. \quad (27b)$$

The formulation for this set of equations is analogous to the formulation presented in Sec. 3. Consider the following pre-dual functional given by

$$\begin{aligned} \hat{S}_H[Y, u, \lambda, \gamma] = & \int_{\Omega} \mathcal{L}(Y, u, \mathcal{D}, x, t) dt dx - \int_0^T f_i(t) \lambda(x, t) dt \Big|_{x=0}^{x=L} \\ & - \int_0^L Y_0(x) \lambda(x, 0) dx - \int_0^T Y_1(t) \gamma(0, t) dt; \quad (28) \end{aligned}$$

$$\mathcal{L}(Y, u, \mathcal{D}, x, t) = -Y \partial_t \lambda + \frac{u^2 \lambda}{2} - Y \partial_x \gamma + \nu u \partial_x \lambda - u \gamma + \frac{\beta_Y}{2} (Y - \bar{Y})^2 + \frac{\beta_u}{2} (u - \bar{u})^2,$$

where  $f_i$ ,  $i = 1, 2$ , are prescribed functions on the left and right boundaries defining natural boundary conditions on those boundaries when  $\lambda$  is allowed to freely vary there. Employing the

following conditions yields the DtP map

$$\frac{\partial \mathcal{L}}{\partial Y} = 0 : \quad Y = Y^{(H)}(\mathcal{D}, x, t) = \bar{Y} + \frac{\partial_t \lambda + \partial_x \gamma}{\beta_Y}; \quad (29a)$$

$$\frac{\partial \mathcal{L}}{\partial u} = 0 : \quad u = u^{(H)}(\mathcal{D}, x, t) = \bar{u} + \frac{\gamma - \lambda \bar{u} - \nu \partial_x \lambda}{\beta_u + \lambda}, \quad (29b)$$

where  $\mathcal{D} := (\lambda, \gamma, \partial_t \lambda, \partial_x \lambda, \partial_x \gamma)$ . Substituting the DtP mapping back into (28) gives us the functional  $S_H[\lambda, \mu]$  which can be explicitly written as

$$\begin{aligned} S_H[\lambda, \gamma] = & \int_{\Omega} \left( -\frac{\mathbb{K}_1}{\beta_Y} (\partial_t \lambda + \partial_x \gamma)^2 - \frac{\mathbb{K}_2}{\beta_u} (\nu \partial_x \lambda + \bar{u} \lambda - \gamma)^2 \right) dt dx \\ & + \int_{\Omega} \left( \bar{Y} (\partial_t \lambda + \partial_x \gamma) + \bar{u} \left( \frac{\lambda \bar{u}}{2} - \gamma + \nu \partial_x \lambda \right) \right) dt dx \\ & - \int_0^L Y_0(x) \lambda(x, 0) dx - \int_0^T Y_l(t) \gamma(0, t) dt, \end{aligned}$$

where

$$\mathbb{K}_1 = \frac{1}{2}; \quad \mathbb{K}_2 = \frac{1}{2 \left( 1 + \frac{\lambda}{\beta_u} \right)},$$

and for  $\beta_u \gg |\lambda|$ ,  $\partial_x \lambda$  now gets penalized (*multiplied by  $\nu$* ). Of course, the E-L equations of  $S_H$  is (27) with the standard substitution of  $(Y, u) \rightarrow (\hat{Y}, \hat{u})$ .

Considering the ellipticity of E-L equations of  $S_H$ , i.e. (27) with the above replacement, the matrix in (21) now has a modification:

$$\mathbb{A}_{1212} = \frac{\nu^2}{\beta_u + \lambda},$$

with the other terms unchanged. Correspondingly, we have

$$c_i A_{ij} c_j = \frac{(c_1 + c_4)^2}{\beta_Y} + \frac{c_2^2 \nu^2}{\beta_u + \lambda} = \frac{(c_1 + c_4)^2}{\beta_Y} + \frac{c_2^2 \nu^2}{\beta_u \left( 1 + \frac{\lambda}{\beta_u} \right)} \quad \forall c \in \mathbb{R}^4.$$

In case when  $\lambda = 0$ , we always have  $c_i A_{ij} c_j \geq 0$  for non-trivial  $c$ . Additionally in a neighborhood of  $\lambda = 0$ , where  $|\lambda| \ll \beta_u$ ,

$$c_i A_{ij} c_j \geq 0 \quad \forall c \in \mathbb{R}^4.$$

This establishes that  $\mathbb{A}_{ijkl}$  is positive semi-definite in this neighborhood and the equation set (27) is locally degenerate elliptic. In contrast to the inviscid Burgers-HJ, the only rank-one matrices along which  $C : \mathbb{A}C = 0$  are of the form  $(0, a_2) \otimes (1, 0)$  for any  $a_2 \in \mathbb{R}$ . Based on the discussion in Sec. 3, it follows that ellipticity is lost only along the normal  $(1, 0)$ , where the first argument represents the component of the normal along the time direction. This is consistent with solutions of Burgers equation ( $\nu \neq 0$ ) as spatial discontinuities in  $u$  are not allowed. The only discontinuity allowed is in  $\partial_t \gamma$  across space-like surfaces ( $t = \text{constant}$ ) but the DtP mapping equations (29) shows that this does not affect  $u^{(H)}$  and hence the mapped primal solutions are continuous; a similar conclusion was also obtained in our dual formulation for the heat equation (see-[1, Sec. 5]).

Similar to the inviscid case, we obtain the following side conditions:

$$\hat{Y}(x, 0) = Y_0(x); \quad \hat{Y}(0, t) = Y_l(t) \quad (30)$$

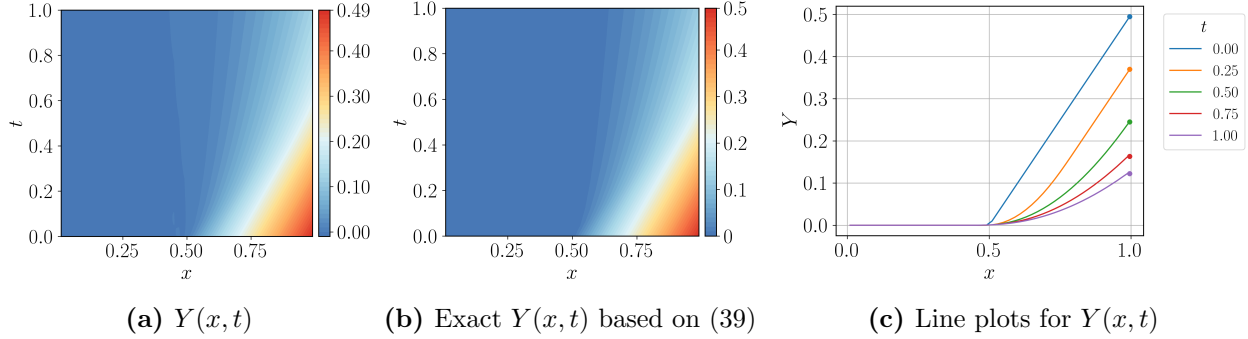


**Figure 13:** DtP mapping generated primal field  $Y$  for the fan example with  $\nu = 10^{-3}$ . In Fig.(c), the dots in various colors at last spatial Gauss point correspond to the exact value of  $Y$  derived from (39), corresponding to the time indicated by the color of each respective dot.

where  $\hat{Y} = Y^{(H)}(\mathcal{D}(x, t), x, t)$ . Additionally, on each of the boundaries, the following operation can be performed which lead to different classes of boundary conditions and hence different problem setups:

- $\lambda$  can be specified as a Dirichlet BC with a fixed arbitrary value. In such a case,  $\delta\lambda = 0$  on the boundary under consideration and we obtain (30) as the only natural b.cs.
- If  $\lambda$  is not specified and allowed to vary freely, then an extra natural BC for  $S_H$ ,

$$\nu \hat{u} = f_i$$

emerges, corresponding to the boundary under consideration.

Our focus is primarily on observing the effect of the  $\nu$  term in the bulk of the domain. Accordingly, we consider the second BC above, weakly enforcing  $u = 0$  on both ends. The impact of this term on the boundaries becomes more pronounced for higher values of  $\nu$ , and we want to operate with as small a value of  $\nu$  as possible. In the following, we show calculations for  $\nu = 10^{-3}$  for the Fan, the Half N-wave and the N-wave problems.

The residual (22) and Jacobian (25) and their corresponding discrete versions are now appropriately modified.

### 5.3.1 Fan

Considering 5.2.1 with an active  $\nu$ , the outcomes are presented in Fig. 13. It is apparent from the figure that the results have exhibited enhancement and closely resemble the exact outcomes of the inviscid case. Upon close inspection, a slight deviation from the exact expression can be noticed close to the right boundary. This discrepancy can be attributed to the influence of an active  $\nu$  and more specifically, to the natural imposition of  $\nu u = 0$  on that boundary.

### 5.3.2 Half N-wave

Considering 5.2.4 again with an active  $\nu$  term, the results as shown in Fig. 14. The boundary effects in this problem are not very pronounced because the Half N-wave itself has a value of  $u = 0$  on the right boundary for a significant duration based on the exact expression. With a small viscosity  $\nu$ , one would not anticipate the solution for this problem to be significantly different from the case where  $\nu = 0$ , which is also evident from the results presented.

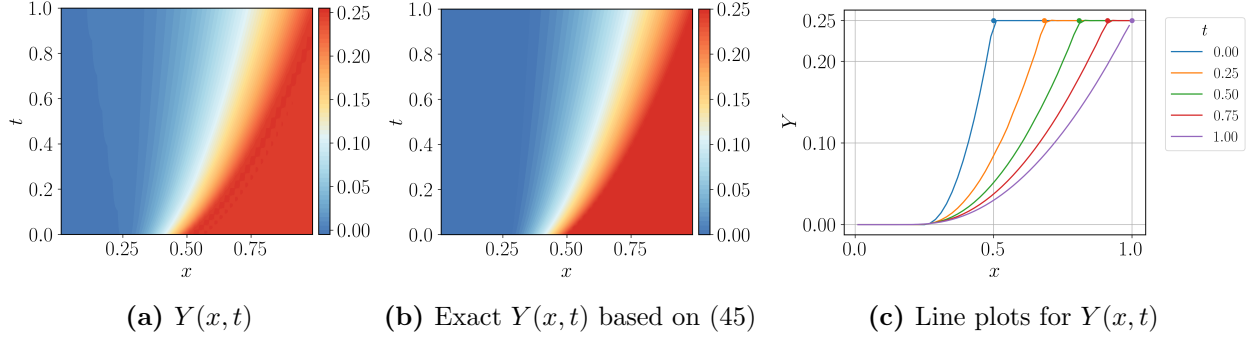


**Figure 14:** DtP mapping generated primal field  $Y$  for the Half N-wave with  $\nu = 10^{-3}$ . In Fig.(c), the coloured dots at  $Y = 0.25$  represent the trajectory of the kink in the space-time domain based on the exact expressions (43) for  $\nu = 0$ .

### 5.3.3 N-wave

Considering the problem 5.2.5 again with an active  $\nu$ , the results are presented in 15, from which it is evident that the two dips have been resolved. Furthermore, the line plots for  $Y$  derived from the  $L^2$  projected data at different nodal times are displayed, revealing the existence of a kink at the node located at  $x = 0.5$ . A slight deviation in the speed at which the kink travels down from the exact expression may again be attributed to the presence of an active  $\nu$ .

## 5.4 Inviscid Burgers-HJ with Viscous base states

In this section we will explore solutions to the inviscid Burgers-HJ equation generated from the dual scheme with base states provided from exact solutions to the (viscous) Burgers-HJ equation with small viscosity.

Given an initial condition  $u_0(x)$  for the Burgers equation, for  $x \in \mathbb{R}$ , the Hopf-Cole transformation can be used to derive the exact expression for  $u(x, t)$  [11] along with its antiderivative with respect to  $x$ ,  $Y(x, t)$ , such that for  $t > 0$  and  $x \in \mathbb{R}$ ,

$$Y(x, t) = -2\nu \log \left[ \frac{1}{2\sqrt{\pi\nu t}} \int_{-\infty}^{\infty} e^{-\frac{Y_0(y)}{2\nu} - \frac{(x-y)^2}{4\nu t}} dy \right]; \quad (31a)$$

$$u(x, t) = \frac{\int_{-\infty}^{\infty} \frac{x-y}{t} e^{-\frac{(x-y)^2}{4\nu t} - \frac{Y_0(x)}{2\nu}} dy}{\int_{-\infty}^{\infty} e^{-\frac{(x-y)^2}{4\nu t} - \frac{Y_0(x)}{2\nu}} dy}, \quad (31b)$$

where  $Y_0$  can be generated via

$$Y_0(x, t) = \int_0^x u_0(y, t) dy$$

and we set  $Y_0(0) = 0$  without loss of generality. These expressions will be denoted as the ‘viscous’ formulae.

For  $\nu \rightarrow 0$ , the formula (31) for  $u(x, t)$  recovers the solution to the inviscid Burgers equation. Motivated by this fact, we set a small value  $\nu = 10^{-3}$  and generate the solutions to the Burgers equation using the expressions (31). We consider the algorithm presented for the Burgers equation (Sec. 5.1) and use the same settings as used for the Half N-wave (Sec. 5.1.4), except that the base state for  $u$  is now set based the expression obtained using the formula (31b). The result for such a setup is shown in Fig. 16a. Similarly for the Burgers-HJ, we utilize the algorithm on the





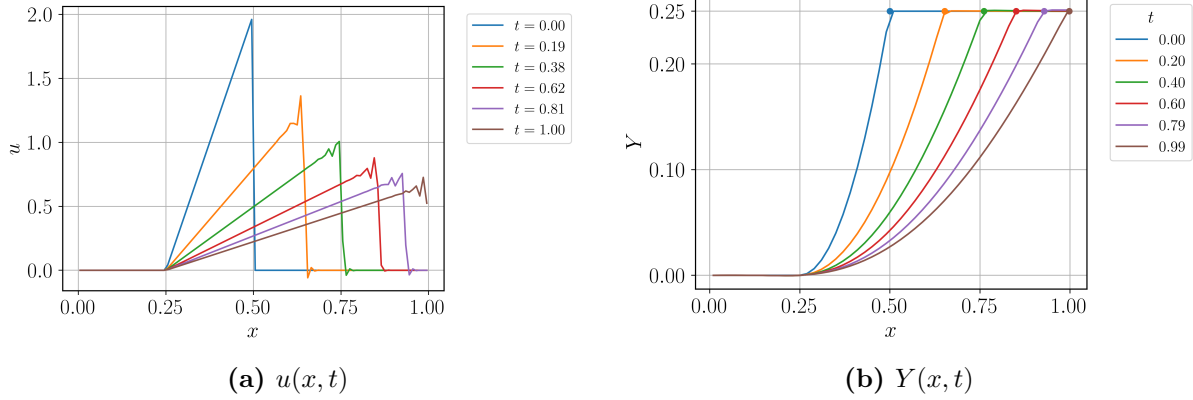


**Figure 16:** (a) is obtained from the formulation based on the Burgers equation Sec. 5.2. (b) is produced using the formulation based on Burgers-HJ Sec. 5.1. Respective base states used for both the problems are based on the viscous formulas (31).

part of the Trimester Program on Mathematics for Complex Materials. The support and hospitality of both institutions is acknowledged.

## Appendices

### A Review of the general formalism

The following two subsections are excerpted from [8, 6] to make this paper self-contained.

#### A.1 The essential idea: An optimization problem for an algebraic system of equations

Consider a generally nonlinear system of algebraic equations in the variables  $x \in \mathbb{R}^n$  given by

$$A_\alpha(x) = 0, \quad (32)$$

where  $A : \mathbb{R}^n \rightarrow \mathbb{R}^N$  is a given function (a simple example would be  $A_\alpha(x) = \bar{A}_{\alpha i} x^i - b_\alpha$ ,  $\alpha = 1 \dots N, i = 1 \dots n$ , where  $\bar{A}$  is a constant matrix, *not necessarily symmetric* (when  $n = N$ ), and  $b$  is a constant vector). We allow for all possibilities  $0 < n \leq N > 0$ .

The goal is to construct an objective function whose critical points solve the system (32) (when a solution exists) by defining an appropriate  $x^* \in \mathbb{R}^n$  satisfying  $A_\alpha(x^*) = 0$ .

For this, consider first the auxiliary function

$$\hat{S}_H(x, z) = z^\alpha A_\alpha(x) + H(x)$$

(where  $H$  belongs to a class of scalar-valued function to be defined shortly) and define

$$S_H(z) = z^\alpha A_\alpha(x_H(z)) + H(x_H(z))$$

with the requirement that the system of equations

$$z^\alpha \frac{\partial A_\alpha}{\partial x^i}(x) + \frac{\partial H}{\partial x^i}(x) = 0 \quad (33)$$

be solvable for the function  $x = x_H(z)$  through the choice of  $H$ , and *any* function  $H$  that facilitates such a solution qualifies for the proposed scheme.

In other words, given a specific  $H$ , it should be possible to define a function  $x_H(z)$  that satisfies

$$z^\alpha \partial_{x^i} A_\alpha(x_H(z)) + \partial_{x^i} H(x_H(z)) = 0 \quad \forall z \in \mathbb{R}^N$$

(the domain of the function  $x_H$  may accommodate more intricacies, but for now we stick to the simplest possibility). Note that (33) is a set of  $n$  equations in  $n$  unknowns regardless of  $N$  ( $z$  for this argument is a parameter).

Assuming this is possible, we have

$$\frac{\partial S_H}{\partial z^\beta}(z) = A_\beta(x_H(z)) + \left( z^\alpha \frac{\partial A_\alpha}{\partial x^i}(x_H(z)) + \frac{\partial H}{\partial x^i}(x_H(z)) \right) \frac{\partial x_H^i}{\partial z^\beta}(z) = A_\beta(x_H(z)),$$

using (33). Thus,

- if  $z_0$  is a critical point of the objective function  $S_H$  satisfying  $\partial_{z^\beta} S_H(z_0) = 0$ , then the system  $A_\alpha(x) = 0$  has a solution defined by  $x_H(z_0)$ ;
- if the system  $A_\alpha(x) = 0$  has a unique solution, say  $y$ , and if  $z_0^H$  is any critical point of  $S_H$ , then  $x_H(z_0^H) = y$ , for all admissible  $H$ .
- If  $A_\alpha(x) = 0$  has non-unique solutions, but  $\partial_{z^\beta} S(z) = 0$  ( $N$  equations in  $N$  unknowns) has a unique solution for a specific choice of the function  $z \mapsto x_H(z)$  related to a choice of  $H$ , then such a choice of  $H$  may be considered a selection criterion for imparting uniqueness to the problem  $A_\alpha(x) = 0$ .
- Finally, to see the difference of this approach with the Least-Squares (LS) Method, we note that the optimality condition for the objective  $A_\alpha(x)A_\alpha(x)$  is  $A_\alpha(x)\partial_{x^i}A_\alpha(x) = 0 \not\Rightarrow A_\alpha(x) = 0$ .

For a linear system  $\bar{A}x = b$ , the LS governing equations are given by

$$\bar{A}^T \bar{A}z = \bar{A}^T b,$$

with LS solution defined as  $z$  even when the original problem  $\bar{A}x = b$  does not have a solution (i.e., when  $b$  is not in the column space of  $\bar{A}$ ). The LS problem always has a solution, of course. In contrast, in the present duality-based approach with quadratic  $H(x) = \frac{1}{2}x^T x$  the governing equation is

$$-\bar{A}\bar{A}^T z = b$$

with solution to  $\bar{A}x = b$  given by  $x = -\bar{A}^T z$ , and the problem has a solution only when  $\bar{A}x = b$  has a solution, since the column spaces of the matrices  $\bar{A}$  and  $\bar{A}\bar{A}^T$  are identical.

## A.2 The idea behind the general formalism

The proposed scheme for generating variational principles for nonlinear PDE systems may be abstracted as follows: We first pose the given system of PDE as a *first-order* system (introducing extra fields representing (higher-order) space and time derivatives of the fields of the given system); as before let us denote this collection of primal fields by  $U$ . ‘Multiplying’ the primal equations by dual Lagrange multiplier fields, the collection denoted by  $D$ , adding a function  $H(U)$ , solely in the variables  $U$  (the purpose of which, and associated requirements, will be clear shortly), and

integrating by parts over the space-time domain, we form a ‘mixed’ functional in the primal and dual fields given by

$$\widehat{S}_H[U, D] = \int_{[0, T] \times \Omega} \mathcal{L}_H(\mathcal{D}, U) dt dx$$

where  $\mathcal{D}$  is a collection of local objects in  $D$  and at most its first order derivatives. We then require that the family of functions  $H$  be such that it allows the definition of a function  $U_H(\mathcal{D})$  such that

$$\frac{\partial \mathcal{L}_H}{\partial U}(\mathcal{D}, U_H(\mathcal{D})) = 0$$

so that the *dual* functional, defined solely on the space of the dual fields  $D$ , given by

$$S_H[D] = \int_{[0, T] \times \Omega} \mathcal{L}_H(\mathcal{D}, U_H(\mathcal{D})) dt dx$$

has the first variation

$$\delta S_H = \int_{[0, T] \times \Omega} \frac{\partial \mathcal{L}_H}{\partial \mathcal{D}} \delta \mathcal{D} dt dx.$$

By the process of formation of the functional  $\widehat{S}_H$ , it can then be seen that the (formal) E-L equations arising from  $\delta S_H$  have to be the original first-order primal system, with  $U$  substituted by  $U_H(\mathcal{D})$ , regardless of the  $H$  employed.

Thus, the proposed scheme may be summarized as follows: we wish to pursue the following (local-global) critical point problem

$$\text{extremize}_D \int_{[0, T] \times \Omega} \text{extremize}_U \mathcal{L}_H(\mathcal{D}(t, x), U) dt dx,$$

where the pointwise extremization of  $\mathcal{L}_H$  over  $U$ , for fixed  $\mathcal{D}$ , is made possible by the choice of  $H$ .

Furthermore, assume the Lagrangian  $\mathcal{L}_H$  can be expressed in the form

$$\mathcal{L}_H(\mathcal{D}, U) := -P(\mathcal{D}) \cdot U + f(U, \mathcal{D}) + H(U)$$

for some function  $P$  defined by the structure of the primal first-order system ((linear terms in) first derivatives of  $U$  after multiplication by the dual fields and integration by parts always produce such terms), and for some function  $f$  which, when non-zero, does not contain any linear dependence in  $U$ . Our scheme requires the existence of a function  $U_H$  defined from ‘solving  $\frac{\partial \mathcal{L}}{\partial U}(\mathcal{D}, U) = 0$  for  $U$ ,’ i.e.  $\exists U_H(P(\mathcal{D}), \mathcal{D})$  s.t. the equation

$$-P(\mathcal{D}) + \frac{\partial f}{\partial U}(U_H(P(\mathcal{D}), \mathcal{D}), \mathcal{D}) + \frac{\partial H}{\partial U}(U_H(P(\mathcal{D}), \mathcal{D})) = 0$$

is satisfied. This requirement may be understood as follows: define

$$f(U, \mathcal{D}) + H(U) =: M(U, \mathcal{D})$$

and assume that it is possible, through the choice of  $H$ , to make the function  $\frac{\partial M}{\partial U}(U, \mathcal{D})$  *monotone* in  $U$  so that a function  $U_H(P, \mathcal{D})$  can be defined that satisfies

$$\frac{\partial M}{\partial U}(U_H(P, \mathcal{D}), \mathcal{D}) = P, \quad \forall P.$$

Then the Lagrangian is

$$\mathcal{L}(\mathcal{D}, U_H(P(\mathcal{D}), \mathcal{D})) = -P(\mathcal{D}) \cdot U_H(P(\mathcal{D}), \mathcal{D}) + M(U_H(P(\mathcal{D}), \mathcal{D}), \mathcal{D}) =: -M^*(P(\mathcal{D}), \mathcal{D})$$

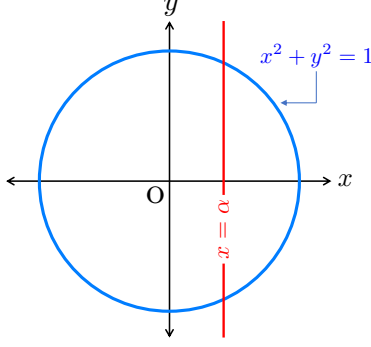


**Figure 17:** Schematic of Circle-line intersection.

where  $M^*(P, \mathcal{D})$  is the Legendre transform of the function  $M$  w.r.t  $U$ , with  $\mathcal{D}$  considered as a parameter.

Thus, our scheme may also be interpreted as designing a concrete realization of abstract saddle point problems in optimization theory [12], where we exploit the fact that, in the context of ‘solving’ PDE viewed as constraints implemented by Lagrange multipliers to generate an unconstrained problem, there is a good deal of freedom in choosing an objective function(al) to be minimized. We exploit this freedom in choosing the function  $H$  to develop dual variational principles corresponding to general systems of PDE.

## B Application of base states: a simple example

Consider the following algebraic system of equations for  $(x, y) \in \mathbb{R}^2, \alpha \in \mathbb{R}$ :

$$\begin{aligned} x^2 + y^2 &= 1 \\ x &= \alpha. \end{aligned} \tag{34}$$

A schematic is shown in Fig. 17, and solutions are given by  $\{(\alpha, \pm\sqrt{1 - \alpha^2}) : |\alpha| \leq 1\}$ . We use the logic of Appendix A.1 to multiply each of the above equations by a dual multiplier and add a quadratic auxiliary potential  $H$ :

$$\widehat{S}(x, y, \lambda, \gamma) = \lambda(x^2 + y^2 - 1) + \gamma(x - \alpha) + \frac{1}{2}(x - \bar{x})^2 + \frac{1}{2}(y - \bar{y})^2,$$

where  $\bar{x}, \bar{y} \in \mathbb{R}$  are constants (in this algebraic problem), and we will refer to the pair as a ‘base state.’ Next we need to generate the analog of the mapping function  $x_H$  of Appendix A.1, also referred to as the DtP mapping in the text:

$$\begin{aligned} \frac{\partial S}{\partial x} = 0 : \quad 2\lambda x + \gamma + (x - \bar{x}) &= 0 \quad \Rightarrow \quad \text{for } \lambda \neq -\frac{1}{2}, \quad x_H(\lambda, \gamma) = \frac{\bar{x} - \gamma}{2\lambda + 1}; \\ \frac{\partial S}{\partial y} = 0 : \quad 2\lambda y + (y - \bar{y}) &= 0 \quad \Rightarrow \quad \text{for } \lambda \neq -\frac{1}{2}, \quad y_H(\lambda) = \frac{\bar{y}}{2\lambda + 1}. \end{aligned} \tag{35}$$

$\lambda \neq -\frac{1}{2}$ : Considering only the case  $\lambda \neq -\frac{1}{2}$  for the moment, the dual objective function is now obtained by substituting the DtP mapping into  $\widehat{S}$ :

$$S(\lambda, \gamma) = \lambda(x_H^2(\lambda, \gamma) + y_H^2(\lambda, \gamma) - 1) + \gamma(x_H(\lambda, \gamma) - \alpha) + \frac{1}{2}(x_H(\lambda, \gamma) - \bar{x})^2 + \frac{1}{2}(y_H(\lambda, \gamma) - \bar{y})^2.$$

The critical point equations for this objective, by design, are the equations (34) with the substitution ( $x \rightarrow x_H, y \rightarrow y_H$ ):

$$\begin{aligned} \frac{(\bar{x} - \gamma)^2}{(2\lambda + 1)^2} + \frac{\bar{y}^2}{(2\lambda + 1)^2} &= 1 \\ \frac{\bar{x} - \gamma}{2\lambda + 1} &= \alpha. \end{aligned}$$

A necessary condition for solutions is

$$(2\lambda + 1)^2(1 - \alpha^2) - \bar{y}^2 = 0$$

which implies that dual solutions exist only for  $|\alpha| \leq 1$  and when  $|\alpha| = 1$  only if  $\bar{y} = 0$ .

Thus, for  $|\alpha| < 1, \bar{y} \neq 0$ ,

$$\lambda = \frac{1}{2} \left( \pm \frac{|\bar{y}|}{\sqrt{1 - \alpha^2}} - 1 \right); \quad \gamma = \bar{x} - \alpha(2\lambda + 1).$$

are the extrema of  $S$ .

Since only  $\lambda \neq -\frac{1}{2}$  is being considered, we do not consider the case  $|\alpha| < 1, \bar{y} = 0$  here.

For  $|\alpha| = 1, \bar{y} = 0$ , the pairs

$$-\frac{1}{2} \neq \lambda \in \mathbb{R} \text{ arbitrary}; \quad \gamma = \bar{x} - \alpha(2\lambda + 1).$$

are the extrema of  $S$ .

Putting these dual solutions back into the DtP mapping (35), we recover the correct primal solutions as expected.

$\lambda = -\frac{1}{2}$ : When  $\lambda = -\frac{1}{2}$ , extrema of  $S$  exist only for  $\bar{y} = 0$  and are given by  $(\lambda = -\frac{1}{2}, \gamma = \bar{x})$ . However, note that this class of dual solutions does not define solutions to the primal problem in a non-vacuous manner (i.e. while all primal solutions are admitted, it does not provide specific guidance for generating primal solutions).

The following conclusion can be drawn from this simple, yet non-trivial, example:

- A ‘good’ choice of the auxiliary function can be crucial for the success of the dual scheme in generating solutions to the primal problem. For example, if ‘no base states’ are invoked within this class of quadratic auxiliary functions, i.e.  $(\bar{x}, \bar{y}) = (0, 0)$ , while dual extrema exist, the scheme essentially fails to define primal solutions, except for the case  $|\alpha| = 1$ . And when the latter is the case for the primal problem, then a base state with non-zero  $\bar{y}$  is not feasible for defining dual and primal solutions to the problem.

## C $L^2$ projection

Let  $u$  represent the primal field under consideration, which may depend on the derivatives of the dual fields (approximated using linear FE shape functions). To achieve a  $C^0$  continuous approximation of  $u$  in the domain  $\Omega \subset \mathbb{R}$  or  $\mathbb{R}^2$ , we employ the following method: Let  $u_h$  represent the projection of  $u$  onto a space  $V_h$  formed by the linear span of globally continuous, piecewise smooth finite element shape functions corresponding to a FE mesh for  $\Omega$ . We enforce the following condition upon  $u_h$ :

$$u_h = \arg \min_{v \in V_h} \int_{\Omega} \frac{1}{2} |u - v|^2 d\Omega.$$

Let  $N^A$  represent the basis functions associated with any node with an index  $A$ . The discrete version of the optimality condition of the above statement is

$$\sum_{A=1}^N \sum_{B=1}^N \delta u_h^A \left( \int_{\Omega} N^A N^B d\Omega \right) u_h^B = \sum_{A=1}^N \delta u_h^A \int_{\Omega} N^A u d\Omega, \quad (36)$$

where  $u_h^B$  denotes the nodal value at node  $B$  of the sought continuous projection of  $u$ , and  $\delta u_h := \delta u_h^A N^A$  is a test function. The primal data for the integral in the right hand side of (36) is obtained from the Gauss points of 1-D/2-D element. In solving (36), we impose any known data, e.g. initial and boundary conditions of the primal problem, as known function values  $u_h^A$ , at corresponding nodes  $A$  where the data is known, with  $\delta u_h^A = 0$ . Using the arbitrariness of the remaining ‘free’  $\delta u_h^A$ , we obtain a system of linear equations to solve for the unconstrained nodal values  $u_h^B, B \in \{1, \dots, N\}$ .

If the  $u$  profile of the primal field is required only at a specific time, then conducting a 1-D  $L^2$  projection along that timeline is advisable since it is computationally inexpensive. As a consequence of  $C^0$  type FE shape functions being employed, the time derivatives of the dual fields experience discontinuities across nodal timelines. In such a case the value of the time derivative on any nodal timeline can be approximated as an average of the value obtained from the element above and below the spatial point of interest (these values remain constant in the direction of time within any element). With the inputs to the DtP mapping generated in this manner, the value of primal fields at the Gauss points (of this nodal timeline) are obtained.

## D The base state smoothing operator

The smoothing operator  $\mathcal{S}$  serves to mitigate the high-wave number contributions in any function. Let  $u := \mathcal{S}[f]$  represent the smoothed output produced for an input function  $f$ . Then we require  $u$  to satisfy:

$$u - \eta \partial_{xx} u = f, \quad \eta > 0. \quad (37)$$

Here,  $\eta$  represents a diffusion-like control parameter.

Let  $t_s$  represent the time at which the smoothing operation occurs. When boundary conditions (BC) are available at  $x = 0$  ( $u_l(t_s)$ ) or (and)  $x = L$  ( $u_r(t_s)$ ) from the primal problem, we employ them as the BCs for  $u$ . However, when the boundary data is not available, we calculate the average of the Gauss data values for the first element ( $f_1^{g1}$  and  $f_1^{g2}$ ) and set it as the left BC, and the average of the Gauss data values for the last element ( $f_l^{g1}$  and  $f_l^{g2}$ ) set it as the right BC on  $u$ . Correspondingly, we generate a weak form for equation (37). Let  $\delta u$  be the space of continuous test functions on  $(0, L)$  with  $\delta u(0) = \delta u(L) = 0$ . The we intend to find  $u$  which satisfies, for such test functions,

$$\int_0^L dx (u \delta u + \eta \partial_x u \partial_x (\delta u) - f \delta u) = 0.$$

We use a standard Galerkin FEM discretization to solve the above with an  $\eta = 10^{-4}$ .

## E Exact entropy solutions for the provided examples

The exact entropy solutions presented in the following examples are based on the concepts and examples outlined in [10]. Given an initial condition  $x \mapsto u_0(x) \in \mathbb{R}$ , entropy solutions to the Burgers equation ( $u$ ) are obtained using two important concepts, recalled below from [10]:

1. Rankine-Hugoniot/jump condition: This is simply a consequence of the underlying conservation statement for Burgers equation as well as looking for weak solutions (in the sense of distributions) to it. If the solution to  $\partial_t u + \partial_x \left( \frac{u^2}{2} \right) = 0$  has different values across a shock curve  $x = X(t)$ , then the shock speed  $s = \frac{dX}{dt}$  must satisfy

$$s = \frac{1}{2} (u(X^+(t)) + u(X^-(t))),$$

where  $X^-$  and  $X^+$  denote the regions immediately to the left and right of the shock, respectively.

2. The Entropy condition: The characteristic lines must go into the shock as  $t$  increases, so those on the left go faster (measured by  $\frac{dX}{dt}$ ) than the shock and those on the right go slower. With respect to the Burgers equation this implies

$$u(X^-(t)) > s > u(X^+(t)).$$

## E.1 Expansion fan

Consider the initial condition

$$u_0(x) = \begin{cases} 0 & \text{for } x < 0.5 \\ 1 & \text{for } x > 0.5. \end{cases}$$

The initial signals for  $x > 0.5$  travel along characteristics with slope 1, while the signals at  $x < 0.5$  travel along vertical characteristics (slope 0, i.e. do not move in space). This leads to an expansion fan filling the space-time in between  $x = 0.5$  and  $x = 0.5 + t$ , which is a rarefaction wave traveling along  $x$ . The corresponding expression for  $u(x, t)$  can then be given as

$$u(x, t) = \begin{cases} 0 & \text{for } x < 0.5 \\ \frac{x - 0.5}{t} & \text{for } 0.5 + t > x \geq 0.5 \\ 1 & \text{for } x \geq 0.5 + t. \end{cases} \quad (38)$$

The corresponding  $Y$  profile for  $Y_0(0) = 0$  is given by

$$Y(x, t) = \begin{cases} 0 & \text{for } x < 0.5 \\ \frac{x^2}{2t} - \frac{0.5x}{t} + \frac{1}{8t} & \text{for } 0.5 + t > x \geq 0.5 \\ x - 0.5 - \frac{t}{2} & \text{for } x \geq 0.5 + t. \end{cases} \quad (39)$$

## E.2 Shock

Consider the initial condition

$$u_0(x) = \begin{cases} 1 & \text{for } x < 0.5 \\ 0 & \text{for } x > 0.5. \end{cases}$$

Given the presence of a jump in the initial condition from 1 to 0 at  $x = 0.5$ , the characteristics originating from the left will merge with the characteristics from the right, resulting in the traveling shock wave with velocity  $s = \frac{1+0}{2} = \frac{1}{2}$ . The exact entropy solution is given by

$$u(x, t) = \begin{cases} 1 & \text{for } x < 0.5 + t/2 \\ 0 & \text{for } x > 0.5 + t/2. \end{cases} \quad (40)$$



The corresponding  $Y$  profile for  $Y_0(0) = 0$  is given by

$$Y(x, t) = \begin{cases} x - \frac{t}{2} & \text{for } x < 0.5 + t/2 \\ 0.5 & \text{for } x > 0.5 + t/2. \end{cases} \quad (41)$$

### E.3 Double shock

Consider the initial condition

$$u_0(x) = \begin{cases} 1 & \text{for } x < 0.25 \\ 0.5 & \text{for } 0.25 < x < 0.5 \\ 0 & \text{for } x > 0.5. \end{cases}$$

Following the same ideas from example E.2, the shock starting at  $x = 0.25$  will travel with a velocity of  $s_1 = \frac{1+0.5}{2} = 0.75$ , while the shock starting at  $x = 0.5$  will travel at with a velocity  $s_2 = \frac{0.5+0}{2} = 0.25$ . Since,  $s_1 > s_2$ , the first shock will merge with the second shock at a time  $t_m$  and travel with a velocity  $s = \frac{1+0}{2} = 0.5$ . The time  $t_m$  for the faster shock to catch up with the slower shock is given by

$$s_1 t_m = s_2 t_m + 0.25 \quad \Rightarrow \quad t_m = 0.5.$$

Consequently the shocks meet at  $x = 0.5 + s_2 t_m = 0.625$ . The solution  $u(x, t)$  is then be given by

$$u(x, t) = \begin{cases} \left. \begin{array}{l} 1 \quad \text{for } x < 0.25 + 0.75t \\ 0.5 \quad \text{for } 0.25 + 0.75t < x < 0.5 + 0.25t \\ 0 \quad \text{for } x > 0.5 + 0.25t \end{array} \right\} t < t_m \\ \left. \begin{array}{l} 1 \quad \text{for } x < 0.625 + 0.5(t - t_m) \\ 0 \quad \text{for } x > 0.625 + 0.5(t - t_m) \end{array} \right\} t > t_m. \end{cases} \quad (42)$$

The corresponding  $Y$  profile for  $Y_0(0) = 0$  is given by

$$Y(x, t) = \begin{cases} \left. \begin{array}{l} x - t/2 \quad \text{for } x < 0.25 + 0.75t \\ x/2 + 0.125 - t/8 \quad \text{for } 0.25 + 0.75t < x < 0.5 + 0.25t \\ 0.375 \quad \text{for } x > 0.5 + 0.25t \end{array} \right\} t < t_m \\ \left. \begin{array}{l} x - t/2 \quad \text{for } x < 0.625 + (t - t_m) \\ 0.375 \quad \text{for } x > 0.625 + (t - t_m) \end{array} \right\} t > t_m. \end{cases} \quad (43)$$

### E.4 Half N-Wave

Consider the initial condition

$$u_0(x) = \begin{cases} 0 & \text{for } x < x_0 \\ \frac{h_0}{l_0}(x - x_0) & \text{for } x_0 \leq x < x_0 + l_0 \\ 0 & \text{for } x > x_0 + l_0. \end{cases}$$

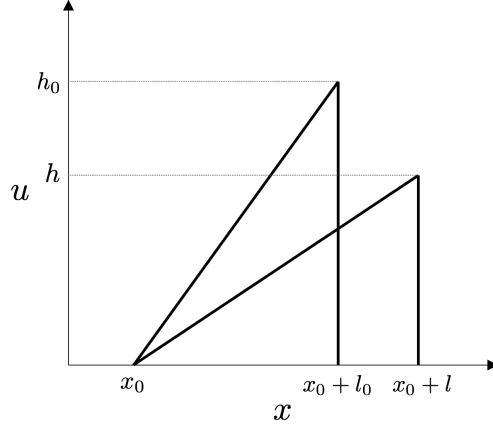


**Figure 18:** The right-angled triangle with a height  $h_0$  indicates the initial profile for the Half N-wave. The right-angled triangle with the height  $h$  indicates the anticipated profile at some later time.

This profile has been depicted in Fig. 18, and it is apparent that the point at  $x = x_0 + l_0$  corresponds to a shock, as  $u_0((x_0 + l_0)^-) > u_0((x_0 + l_0)^+)$ . Furthermore, the point at  $x_0$  serves as a source for an expansion fan due to the linear increase observed from  $x = x_0$  to  $x = x_0 + l_0$ . For any time  $t$ , let the shock be present at a point  $X(t) = x_0 + l(t)$ , where  $l(0) = l_0$  and the height of shock be given by  $h(t)$ , where  $h(0) = h_0$ . To obtain the behavior of the shock front, we utilize the following information:

- Burgers equation on  $\mathbb{R}$  is a conservation law for  $u$  which is conserved:

$$\int_{x_l}^{x_r} \partial_t u \, dx = 0 \quad \Rightarrow \quad \frac{d}{dt} \int_{x_l}^{x_r} u \, dx = 0 \quad \Rightarrow \quad \frac{d}{dt} \int_{x_l}^{x_r} u \, dx = 0$$

for such time that the shock stays with  $[x_l, x_r]$ . This implies

$$\frac{1}{2} h_0 l_0 = \frac{1}{2} h(t) l(t).$$

- Using the Rankine-Hugoniot condition and the last obtained expression across the shock, we establish that

$$s(t) = \frac{dX(t)}{dt} = h(t)/2 \quad \Rightarrow \quad \frac{dl(t)}{dt} = \frac{1}{2} \frac{h_0 l_0}{l(t)}$$

The last expression leads to

$$l(t) = \sqrt{h_0 l_0 t + l_0^2}; \quad X(t) = x_0 + l(t); \quad h(t) = \frac{h_0 l_0}{l(t)}.$$

The solution  $u(x, t)$  is given by

$$u(x, t) = \begin{cases} 0 & \text{for } x < x_0 \\ \frac{h(t)}{l(t)}(x - x_0) & \text{for } x_0 \leq x < x_0 + l(t) \\ 0 & \text{for } x > x_0 + l(t). \end{cases} \quad (44)$$

The corresponding  $Y$  profile for  $Y_0(0) = 0$  is given by

$$Y(x, t) = \begin{cases} 0 & \text{for } x < x_0 \\ \frac{h(t)}{l(t)} \left( \frac{x^2 + x_0^2}{2} - x_0 x \right) & \text{for } x_0 \leq x < x_0 + l(t) \\ \frac{h_0 l_0}{2} & \text{for } x > x_0 + l(t). \end{cases} \quad (45)$$

For the example considered in this paper, we have used the values  $x_0 = 0.25$ ,  $l_0 = 0.25$  and  $h_0 = 2$ .

## E.5 N-wave

Consider the profile given by

$$u_0(x) = \begin{cases} 0 & \text{for } x < 0.25 \\ -4h_0(x - 0.5) & \text{for } 0.25 < x < 0.75 \\ 0 & \text{for } x > 0.75. \end{cases} \quad (46)$$

For the example considered in this paper ( $h_0 = 2$ ), the characteristic plane has been shown in Fig. 19a. Each characteristic ray from  $x^*$  at time  $t = 0$  is a straight line with slope  $u(x^*)$  (Strang, pg. 591 [10]). Accordingly, for any  $x_1, x_2 \in (0.25, 0.75)$ , the characteristics from each of these points will be given by

$$t = \frac{1}{u_0(x_1)}(x - x_1); \quad t = \frac{1}{u_0(x_2)}(x - x_2). \quad (47)$$

Since  $u_0(x)$  is a linearly decreasing function in the considered domain, if  $(x_m, t_m)$  represents the point where two such characteristics meet, substituting (46) into (47) and eliminating  $t_m$  gives

$$-\frac{x_m - x_1}{4h_0(x_1 - 0.5)} = -\frac{x_m - x_2}{4h_0(x_2 - 0.5)} \Rightarrow x_m = 0.5.$$

Using (47),  $t_m = \frac{1}{4h_0}$ . Hence, for linearly decreasing functions  $u_0(x)$ , we find that  $(x_m, t_m)$  is independent of  $x_1$  and  $x_2$  and all such characteristics converge at the single point in space-time. For  $h_0 = 2$ ,  $(x_m, t_m) = (0.5, 0.125)$ .

Beyond  $t = t_m$ , shock formation takes place as a consequence of characteristics traveling in the opposite directions. In the regions  $x < 0.25$  and  $x > 0.75$ , the rays travel parallel to time-axis. Furthermore, the jumps at  $x = 0.25$  and  $x = 0.75$  turn into expansion fans as shown in Fig. 19a. The solution for any point  $\{(x, t) : t > t_m, x \neq 0.5\}$  can be found based on the characteristics coming from the expansion fans. We define the following regions:

$$\begin{aligned} \text{I} &: \{(x, t) : -2t + x - 0.25 \geq 0\} \cap \{(x, t) : 2t + x - 0.75 \leq 0\}; \\ \text{II} &: \{(x, t) : 0.25 \leq x < 0.5\} \cap \{(x, t) : -2t + x - 0.25 \leq 0\}; \\ \text{III} &: \{(x, t) : 0.5 < x \leq 0.75\} \cap \{(x, t) : 2t + x - 0.75 \geq 0\}. \end{aligned}$$

The complete  $u$  profile can thus be given by

$$u(x, t) = \begin{cases} \frac{8(x - 0.5)}{8t - 1} & \text{for Region I} \\ \frac{x - 0.25}{t} & \text{for Region II} \\ \frac{x - 0.75}{t} & \text{for Region III} \\ 0 & \text{Otherwise.} \end{cases} \quad (48)$$

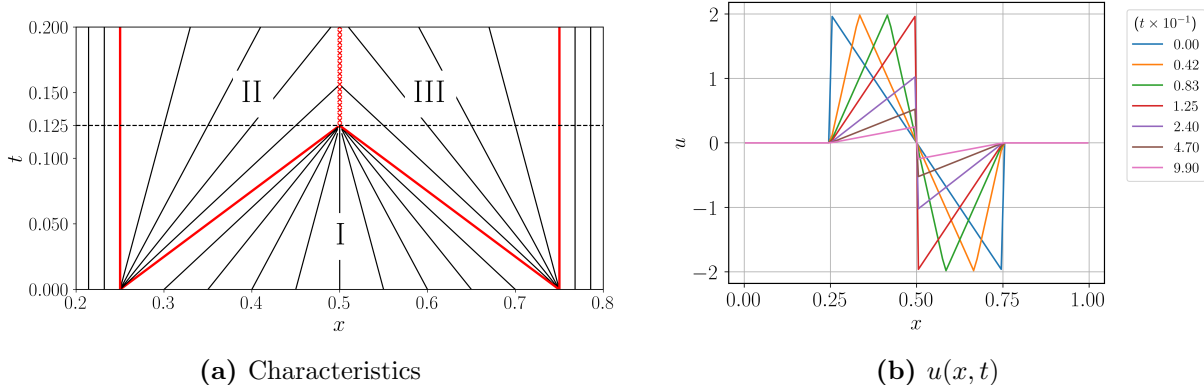


**Figure 19:** In Fig. 19a, slope of any characteristic in the  $x - t$  plane is given by  $1/u(x, t)$ . Three distinct regions are delineated by the red-colored lines. The red coloured, vertical x-patterned line beyond  $t_m$  at  $x = 0.5$  represents the shock.

The continuous  $Y$  profile corresponding to  $Y(0, t) = 0$  can be obtained as

$$Y(x, t) = \left\{ \begin{array}{ll} \frac{2x^2 - x}{4t} + \frac{1}{32t} & \text{for } 0.25 \leq x < 0.25 + 2t \\ \frac{4(x^2 - x)}{8t - 1} + \frac{8t + 3}{4(8t - 1)} & \text{for } 0.25 + h_0 t \leq x < 0.75 - h_0 t \\ \frac{2x^2 - 3x}{4t} + \frac{9}{32t} & \text{for } 0.75 - h_0 t \leq x < 0.75 \\ 0 & \text{Otherwise} \end{array} \right\} \quad 0 < t < t_m \quad (49)$$

$$\left. \begin{array}{ll} \frac{2x^2 - x}{4t} + \frac{1}{32t} & \text{for } 0.25 \leq x < 0.5 \\ \frac{2x^2 - 3x}{4t} + \frac{9}{32t} & \text{for } 0.5 \leq x < 0.75 \\ 0 & \text{Otherwise} \end{array} \right\} t \geq t_m.$$

## References

- [1] U. Kouskiya and A. Acharya, “Hidden convexity in the heat, linear transport, and euler’s rigid body equations: A computational approach.” To appear in Quarterly of Applied Mathematics, <https://arxiv.org/abs/2304.09418>, 2023.
- [2] Y. Brenier, “The initial value problem for the Euler equations of incompressible fluids viewed as a concave maximization problem,” Communications in Mathematical Physics, vol. 364, no. 2, pp. 579–605, 2018.
- [3] —, “Examples of hidden convexity in nonlinear PDEs,” <https://hal.science/hal-02928398/document>, 2020.
- [4] J. M. Burgers, “A mathematical model illustrating the theory of turbulence,” Advances in Applied Mechanics, vol. 1, pp. 171–199, 1948.

- [5] H. Bateman, “Some recent researches on the motion of fluids,” Monthly Weather Review, vol. 43, no. 4, p. 163–170, 1915.
- [6] A. Acharya, “A dual variational principle for nonlinear dislocation dynamics,” Journal of Elasticity, <https://doi.org/10.1007/s10659-023-09998-5>, 2023.
- [7] —, “A hidden convexity in continuum mechanics, with application to classical, continuous-time, rate-(in) dependent plasticity,” arXiv preprint arXiv:2310.03201, 2023.
- [8] —, “Variational principles for nonlinear PDE systems via duality,” Quarterly of Applied Mathematics, vol. LXXXI, pp. 127–140, 2023, Article electronically published on September 26, 2022.
- [9] P. D. Lax, Hyperbolic Systems of Conservation Laws and the Mathematical Theory of Shock Waves. Society for Industrial and Applied Mathematics, 1973.
- [10] G. Strang, Introduction to Applied Mathematics. Wellesley Cambridge Press, 1977.
- [11] T. P. Liu, “Hopf-Cole Transformation,” Academia Sinica (New Series), Bulletin of the Institute of Mathematics, vol. 12, no. 7, pp. 71–101, 2017.
- [12] R. T. Rockafellar, Conjugate duality and optimization. SIAM, 1974.